Rapid auxin-mediated phosphorylation of Myosin regulates trafficking and polarity in Arabidopsis

Huibin Han[1*], Inge Verstraeten[1*], Mark Roosjen[2], Ewa Mazur[3], Nikola Rýdza[4], Jakub Hajný[1,5], Krisztina Ötvös[1,6], Dolf Weijers[2§], Jiří Friml[1§]

[1] Institute of Science and Technology (IST) Austria, Am Campus 1, 3400 Klosterneuburg, Austria

[2] Laboratory of Biochemistry, Wageningen University, Stippeneng 4, 6708WE Wageningen, the Netherlands

[3] Faculty of Natural Sciences, Institute of Biology, Biotechnology and Environmental Protection, University of Silesia in Katowice, Jagiellońska 28, 40-032 Katowice Poland

[4] Central European Institute of Technology, Masaryk University, Kamenice 753/5, 625 00 Brno, Czech Republic

[5] Laboratory of Growth Regulators, The Czech Academy of Sciences, Institute of Experimental Botany & Palacký University, Šlechtitelů 27, CZ-78371 Olomouc, Czech Republic

[6] Current address: Bioresources Unit, Center for Health & Bioresources, AIT Austrian Institute of Technology GmbH, 3430 Tulln, Austria

[*] Authors contributed equally to this publication

[§] Correspondence: jiri.friml@ist.ac.at and dolf.weijers@wur.nl

Abstract (150)

The signaling molecule auxin controls plant development through a well-known transcriptional mechanism that regulates many genes. However, auxin also triggers cellular responses within seconds or minutes, and mechanisms mediating such fast responses have remained elusive. Here, we identified an ultrafast auxin-mediated protein phosphorylation response in Arabidopsis roots that is largely independent of the canonical TIR1/AFB receptors. Among targets of this novel response are Myosin XI and its adaptor protein MadB2. We show that their auxin-mediated phosphorylation regulates trafficking and polar, subcellular distribution of PIN auxin transporters. This phosphorylation-based auxin signaling module is indispensable during developmental processes that rely on auxin-mediated PIN repolarization, such as termination of shoot gravitropic bending or vasculature formation and regeneration. Hence, we identified a fast, non-canonical auxin response targeting multiple cellular processes and revealed auxin-triggered phosphorylation of a myosin complex as the mechanism for feedback regulation of directional auxin transport, a central component of auxin canalization, which underlies self-organizing plant development.

Keywords: auxin signaling, auxin transport, auxin canalization, phosphorylation, myosin, cell polarity, endocytosis, trafficking

Introduction

The plant hormone auxin acts as a key regulator of plant development and controls multiple cellular processes. The current main paradigm of auxin action is that it transcriptionally reprograms individual cell behavior to continually perpetuate and adapt overall plant development (Bargman et al., 2013; Weijers and Wagner, 2016; Lavy and Estelle, 2016). The transcriptional auxin response is complex; numerous genes are controlled by auxin and are differentially expressed across tissues and organs depending on the developmental contexts (Kieffer et al., 2010; Salehin et al., 2015). Transcriptional auxin responses are mediated by the canonical TIR1/AFBs-Aux/IAA-ARF nuclear signaling pathway, which allows changes at the level of RNA in response to auxin in a timeframe of 3 to 5 minutes (McClure et al., 1989; Abel and Theologis, 1996) followed by changes in protein levels and activities at later time points. However, some auxin activities depending on the TIR1/AFB receptors, such as root growth inhibition (Fendrych et al., 2018) and root hair elongation (Dindas et al., 2018) are too fast to involve transcriptional regulation. This implies that TIR1/AFB auxin receptors, besides their well-characterized mechanism of transcriptional regulation, also trigger a so far unknown non-transcriptional signaling branch (Kubeš and Napier, 2019; Gallei et al., 2020).

In decades of auxin research, repeated observations of rapid cellular auxin effects have been made, including plasma membrane (PM) hyperpolarization, H^+-pump activation, cytosolic Ca^{2+} or pH changes and protoplast swelling (Kubeš and Napier 2019). The underlying molecular mechanisms remain a mystery, but due to their rapidness, they were never linked to the canonical TIR1/AFB-Aux/IAA pathway and its downstream transcriptional responses. Prominent among those is the auxin regulation of clathrin-mediated endocytic trafficking of PIN auxin transporters (Adamowski and Friml, 2015; Narasimhan et al., 2020). This effect does not require the TIR1/AFB pathway and is presumably part of the feedback regulation of auxin on its intercellular auxin flow (Paciorek et al., 2005; Robert et al., 2010; Hajny et al., 2020). Moreover, a newly identified auxin analogue Pinstatic acid does not act via TIR1/AFB receptors, but still triggers distinct auxin responses, including the effect on PIN trafficking and auxin transport (Oochi et al., 2019). All these observations support existence of fast auxin responses mediated by so far unknown modes of auxin signaling and perception distinct from the well-studied nuclear TIR1/AFB mechanism (Gallei et al., 2020). Cell surface-localized TMK receptor-like kinases may contribute to this uncharacterized auxin signaling (Cao et al., 2019; Xu et al., 2014; Li, Verstraeten et al., 2021; Lin

69 et al., 2021), but this remains unclear, mainly due to lack of an established auxin perception

70 mechanism for this pathway.

71 Another key aspect of auxin action is directional auxin transport between cells (Vanneste and

72 Friml, 2009). The establishment of auxin gradients and local maxima and minima in plant tissues

73 can be attributed to local auxin biosynthesis (Morffy and Strader, 2020) and directional,

74 intercellular auxin transport (Adamowski and Friml, 2015). Directionality of auxin flow is

75 achieved by action and asymmetric (polarized) cellular localization of PIN auxin exporters at

76 specific cell sides (Petrášek et al., 2006; Wiśniewska et al., 2006). PIN polarity and abundance at

77 the PM depends on vesicle transport-related processes, such as constitutive recycling (Geldner et

78 al., 2001) and clathrin-mediated endocytosis (Dhonukshe et al., 2007; Glanc et al., 2018), *de novo*

79 secretion (Jásik et al., 2016; Salanenka et al., 2018) and degradation in lytic vacuoles (Abas et al.,

80 2006; Kleine-Vehn et al., 2008a). Additionally, PIN phosphorylation at different residues is a key

81 mechanism for PIN polarity or activity regulation (Michniewicz et al., 2007; Zhang et al., 2010;

82 Barbosa et al., 2018; Tan et al., 2020, 2021; Xiao and Offringa, 2020). The cellular dynamics of

83 the PIN-dependent auxin transport network have emerged as a prominent mechanism capable of

84 translating endogenous (e.g. plant hormones) and exogenous (e.g. light and gravity) signals into

85 developmental responses via relocating PIN transporters and thus redirecting routes of auxin

86 transport (Vanneste and Friml, 2009; Adamowski and Friml, 2015).

87 Crucial regulation of PIN-mediated transport is by auxin itself. This positive feedback

88 between auxin signaling and transport directionality is the key pre-requisite of the so-called auxin

89 canalization (Sachs, 1981). The auxin canalization hypothesis proposes a mechanism for unique,

90 self-organizing aspects of plant development such as the establishment of the apical/basal body

91 axis during embryogenesis (Robert et al., 2013, 2018), flexible formation of vascular strands

92 during organ formation (Benková et al., 2003; Heisler et al., 2005; Bhatia et al., 2016), shoot

93 branching (Bennett et al., 2014; Zhang et al., 2020), leaf venation (Scarpella et al., 2006;

94 Govindaraju et al., 2020), vasculature regeneration after wounding (Sauer et al., 2006; Mazur et

95 al., 2016, 2020a; Hajný et al., 2020) and shoot gravitropic bending termination (Rakusová et al.,

96 2016, 2019; Han et al., 2020). During canalization, auxin triggers coordinated PIN polarization to

97 gradually establish directional auxin transport channels between auxin source and sink (Wabnik et

98 al., 2010, 2011; Prát et al., 2018). Genetic and cell biological studies suggest that the auxin effect

99 on PIN endocytic trafficking is central for PIN polarization and canalization (Sauer et al., 2006;

100　Mazur et al., 2020a; Zhang et al., 2020). Nonetheless, auxin signaling mechanisms and

101　downstream cellular processes, by which auxin regulates both PIN polarity and subcellular

102　trafficking crucial for the self-organizing canalization processes, still remain elusive.

103　　Here, we established a phospho-proteomics approach to identify components of the fast, non-

104　transcriptional auxin responses. Among proteins that were rapidly phosphorylated in a TIR1/AFB-

105　dependent and -independent manner, we further characterized the Myosin XI and MadB2 myosin

106　binding proteins. We demonstrate that auxin-mediated phosphorylation of the myosin complex is

107　essential for the feedback regulation of PIN auxin transporter trafficking and polarization, which

108　is ultimately involved in canalization-mediated developmental processes such as vasculature

109　formation in leaves or regeneration of wounded stems. Overall, our study uncovers novel

110　downstream components of a so far elusive rapid auxin action and identifies Myosin XI proteins

111　and their phospho-status as a crucial part of the mechanism, by which auxin regulates its own

112　transport during plant development.

113

Results

Rapid auxin-mediated protein phosphorylation

116　Several responses to auxin occur within minutes or faster, and are too quick to be mediated by

117　gene expression changes (Fendrych et al., 2018; Kubeš and Napier, 2019). Similar rapid responses

118　such as for animal steroid hormones (Steinman and Trainor, 2010), or for osmotic stress in

119　*Arabidopsis* (Stecker et al., 2014) have been attributed to changes in protein phosphorylation as

120　prominent downstream signaling events.

121　　Therefore, we tested whether auxin triggers rapid changes in protein phosphorylation and

122　developed a procedure allowing to detect auxin-mediated phosphorylation events in times shorter

123　than 2 minutes after auxin exposure. To maximize the detection depth for phospho-peptides in

124　plant extracts, we compared a number of protein extraction and phospho-peptide enrichment

125　strategies (**Figure S1A-J**). We found Filter-Aided Sample Preparation (FASP) to yield the best

126　results, identifying most phospho-peptides with the least co-purification of nucleic acids (**Figure

127　S1C**). We next combined FASP with various phospho-peptide enrichment strategies and obtained

128　superior recovery with magnetic Ti^{4+} beads, identifying nearly 1500 phospho-peptides from

129　Arabidopsis root extracts (**Figure S1A-B**). We found a significant overlap between the 3

130　phosphopeptide enrichment methods, but overall the Ti^{4+} beads resulted in the biggest portion of

131 uniquely identified peptides (**Figure S1D**). When compared with the alternative enrichment

132 methods, Ti^{4+} IMAC enrichment did not show a bias for charged peptides and mostly identified

133 phospho-serines and -threonines (**Figure S1E**). TiO$_2$(Mg) MOAC enrichment on the other hand

134 resulted in more acidic phospho-peptides (**Figure S1E,I**). For the three evaluated methods, the

135 overall nature of phosphorylated amino acids followed the previously published distribution:

136 Serine(S) ~90%, Threonine(T) ~7 and Tyrosine(Y) ~1% (Wu et al., 2015) without discernable

137 differences between them (**Figure S1F**). Moreover, also biochemical properties such as

138 hydrophobicity or amino acid length did not differ significantly between the peptide enrichment

139 methods (**Figure S1H-J**). In general, a protocol combining FASP and Ti^{4+} peptide enrichment was

140 the best method for the identification of phospho-peptides in *Arabidospis thaliana* root samples,

141 treated for 2 minutes with 100 nM indole-3-acetic acid (IAA) (**Figure 1A**).

142 Our combined protein extraction and phospho-peptides enrichment method (**Figure 1A**)

143 identified about 3100 phospho-peptides, which were subjected to a sensitive hybrid data analysis

144 approach (Nikonorova et al., 2018) that allows detection of differential abundance across samples

145 despite missing values. After filtering, the 2157 remaining phospho-peptides were subjected to

146 FDR-controlled statistical comparison across treatments, resulting in about 10% differentially

147 abundant phospho-peptides (FDR ≤ 0.05; **Figure 1B**). Global analysis showed that IAA mainly

148 induced phosporylation, while limited auxin-dependent reduction in phosphorylation was detected

149 (**Figure 1B**). The differential phospho-peptides map to 338 proteins (**Supplemental Table S1**)

150 and among these are several proteins for which auxin-mediated phosphorylation has previously

151 been shown (Zhang et al., 2013), such as SNX1 and AHA2 (**Figure 1C**). However, a large portion

152 of the rapidly induced phospho-sites is unique (300/506; **Figure 1C**). Comparison of the proteins

153 that are differentially phosphorylated with transcriptionally regulated genes (Lewis et al., 2013)

154 confirmed that the early auxin-induced phospho-response targets a different and unique set of

155 proteins (**Figure 1D**). Thus, auxin induces a rapid (within 2 minutes or shorter) protein

156 phosphorylation response.

157 We next addressed whether the rapid phosphorylation response is mediated by the TIR1/AFB

158 pathway using either PEO-IAA, an auxin antagonist for TIR1/AFB receptors (Hayashi et al., 2008)

159 or the orthologous cvxIAA/ccvTIR1 system that specifically activates TIR1/AFB signaling

160 (Uchida et al., 2018). Notably, cvxIAA in *ccvTIR1* roots induced some changes in phosphorylation,

161 but the overlap with IAA-induced phosphorylation changes was limited (**Figure 1B, E**),

162 suggesting that a substantial portion of the rapid auxin phospho-response was TIR1-independent

163 (**Figure S2A**). PEO-IAA also rapidly induced changes in phosphorylation (**Figure 1B, E**), but

164 again this phospho-response overlapped minimally with IAA-dependent or TIR1/AFB-dependent

165 phospho-sites (**Figure 1E; Figure S2A-B**). The PEO-IAA treatment and the engineered

166 cvxIAA/*ccvTIR* combination provide independent confirmation that the rapid phospho-response

167 is, to a large extent, independent of the known TIR1/AFB auxin signaling.

168 Thus, we identified a novel, ultrafast auxin response that leads to differential phosphorylation

169 of a range of proteins and is largely mediated through a yet unknown auxin perception mechanism.

170

171 **Auxin-mediated phosphorylation of Myosin XI and Myosin-binding proteins**

172 The 338 proteins rapidly phosphorylated in response to auxin (**Supplemental Table S1**) reside in

173 the nucleus, cytosol and at the PM (**Figure S2C**). The residues targeted by auxin-dependent

174 phosphorylation were mostly serines, which follows the predicted phosphorylation pattern (**Figure**

175 **S2D**; Wu et al., 2015**)**. Among the rapidly phosphorylated proteins following auxin treatment were

176 known regulators of auxin response such as 3-Phosphoinositide-Dependent protein Kinase 1

177 (PDK1), an AGC kinase that activates PIN auxin transporters (Tan et al., 2020; Xiao and Offringa,

178 2020), but the majority of the identified targets were novel. Some have reported roles in membrane

179 trafficking (e.g. SYP132, BIG3, DRP2A/B, EPSIN2), microtubule regulation (e.g. MAP70-1,

180 TOR1, NEK5) or chromatin biology (e.g. SUVR5, TPL, BRM, HDT1), but had not previously

181 been associated with auxin-dependent processes. In short, the phospho-proteome dataset

182 represents a rich starting point for exploring novel fast auxin responses.

183 Among the identified proteins (**Supplemental Table S1**), Myosin XIK (Uniprot code

184 A0A1P8BCY2; encoded by AT5G20490), a motor protein with actin binding capability and

185 presumably involved in endomembrane vesicular transport (Peremyslov et al., 2012), emerged as

186 a prominent candidate phosphorylated in response to IAA treatment in several independent MS

187 experiments (**Figure 2A; Supplemental Table S1**). In the globular tail domain (GTD) of Myosin

188 XIK, the serine at position 1234 (S1234) was phosphorylated following IAA treatment, while

189 phosphorylation of this site was not detected following PEO-IAA treatment and only minor

190 differential phosphorylation was observed with cvxIAA treatment in *ccvTIR1* roots (**Figure 2A**),

191 both suggesting largely TIR1/AFB-independent phosphorylation. We thus decided to

192 independently confirm *in vivo*, auxin-mediated phosphorylation of the globular tail of Myosin XIK

193   (S1234) by Western blot. To this end, we fused the GTD of myosin XIK with an RFP-tag and

194   expressed the construct under the 35S promoter (*35S::MyosinXIK^{WT}* hereafter called *XIK^{WT}*). This

195   constructs were transformed into both, WT (Col-0) background and stable transformed seedlings

196   were treated with 10 µM of synthetic auxin, 1-napththalene-acetic acid (NAA) for 30 minutes. Our

197   Phos-tag Western blot analysis confirmed that Myosin XIK was more phosphorylated following

198   auxin treatment (**Figure 2C**).

199   The *Arabidopsis* genome encodes 17 Myosin family members that are highly conserved

200   (Reddy et al., 2001; Avisar et al., 2009; Ryan et al., 2017). Myosins have been shown to play roles

201   in vesicle trafficking and endocytosis (Prokhnevsky et al., 2008; Peremyslov et al., 2012),

202   gravitropism (Okamoto et al., 2015; Talts et al., 2016), auxin transport (Abu-Abied et al., 2018)

203   and response (Ojangu et al., 2018). Protein alignment revealed that the S1234 phospho-site is

204   conserved in Myosin XI proteins (**Figure S3A**). Despite not detected in the phospho-dataset,

205   disruption of the homologous Myosin XIF, which is highly expressed in roots, results in similar

206   trafficking defects (Avisar et al., 2008; Haraguchi et al., 2018). Therefore, we focused on both

207   these close homologues, Myosin XIF and XIF.

208   Furthermore, we found Myosin binding protein MadB2/CLMP1/PHOX2 (AT1G62390) to be

209   hyperphosphorylated following auxin treatment (**Figure 2B**). MadB2 has been shown to bind to

210   Myosin XIK, but its function in plant development is less characterized (Kurth et al., 2017).

211   Thus, auxin induces rapid phosphorylation of Myosin XIK and the associated MadB2. This

212   suggests that the identified ultrafast rapid auxin signaling targets myosin and associated proteins,

213   thereby providing a potential mechanism to rapidly regulate cellular processes including auxin

214   transport.

215

216   **Myosins XI in auxin-sensitive endomembrane PIN trafficking**

217   Dynamic polar localization and thus action of PIN auxin transporters is tightly regulated by

218   constitutive endocytic trafficking between PM and endosomes, which is actin-dependent (Geldner

219   et al., 2001; Kleine-Vehn et al., 2008b) and thus potentially linked with myosin motor proteins

220   function (Peremyslov et al., 2012). Furthermore, auxins, chiefly NAA, interfere with this PIN

221   endocytic recycling providing a possible mechanism for feedback regulation of auxin transport

222   (Narasimhan et al., 2020; Wabnik et al., 2011). We hence tested the involvement of Myosin XI

223   proteins and their auxin-mediated phosphorylation in endocytic trafficking of PIN proteins, in

224   particular.

225   Constitutive endocytic recycling of PIN proteins can be indirectly visualized by intracellular

226   aggregation following treatment with the trafficking inhibitor Brefeldin A (BFA) (Geldner et al.,

227   2001). After BFA treatment, the *myosin xik xif* double mutant displayed less intracellular PIN1

228   aggregation into so-called BFA bodies than the wild type (WT) (**Figure 3A-B**) implying defective

229   PIN1 endocytic trafficking in the *myosin xik xif* mutant. Whereas in WT roots, NAA significantly

230   reduced BFA body formation (Paciorek et al., 2005), we did not observe any such effects in *myosin*

231   *xik xif* roots (**Figure 3A-B**).

232   To asses a role of Myosin XI proteins in general trafficking, we followed the uptake of the

233   lipophilic FM4-64 dye, which incorporates in the PM and gets into the cell by internalization to

234   gradually mark endomembranes (Jelínková et al., 2010). Quantification of cytoplasmic (CM)

235   FM4-64 staining and the PM-retained signal, revealed that FM4-64 uptake is significantly reduced

236   in *myosin xik xif* mutants compared to WT (**Figure 3C-D**). Moreover, whereas NAA-treatment

237   strongly reduced the internalization of FM4-64 in WT roots, we did not observe any additional

238   effects of NAA in *myosin xik xif* roots (**Figure 3C-D**).

239   These observations demonstrate that Myosins XI are required for endomembrane trafficking

240   and more specifically for the PIN1 endocytic recycling. Furthermore, the auxin-insensitivity of the

241   *myosin* mutants in terms of PIN trafficking and global endocytosis indicates that the Myosin XI

242   function may be required for the auxin-regulation of these trafficking processes.

243

Auxin-mediated Myosin XI phosphorylation in endomembrane and PIN trafficking

244

245   Involvement of Myosin XI in auxin regulation of trafficking and its rapid auxin-triggered

246   phosphorylation (**Figure 2**) prompted us to test the physiological relevance of the S1234 or S1256

247   phosphorylation in Myosin XIK and Myosin XIF,dv respectively. In the globular tail sequence,

248   we mutated the respective Serine to Alanine to prevent phosphorylation (*MyosinXIK^{S1234A}* and

249   *MyosinXIF^{S1256A}*). Mutated sequences were C-terminally fused with an RFP-encoding tag,

250   expressed under a *35S* promoter and introduced into WT (Col-0) and *myosin xik xif* mutant plants.

251   Homozygous seedlings expressing the phospho-deficient Myosin XIK and XIF constructs (in Col-

252   0 background) were treated with 10 µM NAA for 30 minutes to verify the phosphorylation status

253   of Myosin XIK and XIF proteins in these mutants. Phos-tag and normal Western blot analysis

254 showed that the phospho-deficient mutants were not phosphorylated following auxin treatment
255 (**Figure S4A-C**).

256   We next examined whether the phosphorylation status of Myosin XIK and XIF contributes to
257 regulation of PIN trafficking. When introduced into WT plants, the phospho-deficient mutants
258 (*35S::MyosinXIK*^{S1234A} and *35S::MyosinXIF*^{S1256A}, hereafter *XIK*^{S1234A} and *XIF*^{S1256A}) showed less
259 intracellular PIN1 aggregation in BFA bodies (**Figure 4A-B; Figure S4D**), less FM4-64 uptake
260 (**Figure 4C-D; Figure S4E**) and were also less sensitive to auxin treatment (**Figure 4A-D; Figure**
261 **S4D,E**). When introduced into the *myosin xik xif* mutant, the *XIK*^{WT} and *XIF*^{WT} constructs
262 complemented the defective PIN1 accumulation in the BFA bodies (**Figure S5A-C**) and FM4-64
263 uptake (**Figure S5D-F**), whereas the phospho-deficient Myosin XI constructs were unable to
264 rescue these defects (**Figure S5**).

265   Taken together, our results revealed that auxin-mediated phosphorylation of serine residues
266 in the globular tail of Myosin XI proteins is critical for their function in auxin-sensitive
267 endomembrane and PIN trafficking.

268

269 **Auxin-mediated Myosin XI phosphorylation in PIN1 repolarization in roots**
270 The physiological relevance of auxin regulation of PIN endocytic trafficking is unclear. It has been
271 proposed to be a key part of the cellular mechanism for auxin feedback on auxin transport and its
272 directionality. This, in turn, is an essential pre-requisite of auxin canalization, a process allowing
273 for the self-organized formation of polarized auxin channels during many developmental processes
274 (Wabnik et al., 2010, 2011). Indeed, genetic and pharmacological manipulations revealed the
275 crucial importance of auxin-regulated trafficking for auxin effect on PIN polarity and for formation
276 of auxin transporting channels (Mazur et al., 2020a; Zhang et al., 2020; Hajný et al., 2020).

277   Therefore, we tested the involvement of Myosin XI in the auxin effect on PIN polarity, which
278 can be visualized by PIN1 repolarization in auxin-treated roots (Sauer et al., 2006; Prát et al., 2018).
279 As seen before, auxin induced a relocalization of PIN1 from the basal to the inner lateral side of
280 endodermal cells in WT roots (**Figure 5A-C**) but, importantly, this auxin effect was not observed
281 in the *myosin xik xif* mutant roots (**Figure 5A-C**). These observations demonstrate importance of
282 Myosin XI for auxin-regulation of PIN polarity.

283   We then tested the ability of auxin to promote PIN1 repolarization in Myosin XI phospho-
284 deficient mutants (in WT background). Our results showed that the phospho-deficient mutants

285   were auxin-insensitive (**Figure 5A-C, Figure S6A**). Additionally, the defective auxin-mediated

286   PIN1 repolarization in *myosin xik xif* mutants was rescued by introducing the non-mutated

287   constructs (XIF^{WT} and XIK^{WT}), but not by the phospho-deficient constructs (XIF^{S1256A} and XIK^{S1234A})

288   (**Figure S6B-D**).

289   These results show that the Myosin XI function is required for auxin-mediated PIN

290   repolarization in roots and that auxin-mediated phosphorylation of the serine residue in its globular

291   tail is critical for the function in mediating auxin effect on PIN1 polarity.

292

293   **MadB2 myosin binding proteins in auxin-mediated regulation of trafficking and PIN**

294   **polarity**

295   Auxin induced phosphorylation not only of Myosin XI, but also of MadB2 Myosin binding

296   proteins (**Figure 2B; Supplemental Table S1**). MadB2 has been shown to directly interact with

297   Myosin XIK and it redundantly acts with its three paralogs in root hair growth (Kurth et al., 2017).

298   We examined whether MadB2 function is required for regulation of PIN polarity and

299   trafficking. Following BFA treatment, *madb2* quadruple mutant (*madb 4KO*) accumulated less

300   PIN1 in BFA bodies and also showed decreased sensitivity to auxin treatment (**Figures S7A**).

301   Quantification of FM4-64 uptake demonstrated that endomembrane trafficking was also impaired

302   in *madb 4KO* mutants and auxin treatment showed no additional inhibitory effect (**Figures S7B**).

303   We also tested auxin-mediated PIN1 lateralization in *madb 4KO* mutant roots. Again, auxin failed

304   to repolarize PIN1 to the lateral side of endodermal cells in *madb 4KO* roots (**Figure S7C**).

305   In conclusion, loss-of-function mutants in Myosin XI and in MadB2 Myosin binding proteins

306   show essentially identical defects in auxin-regulated PIN trafficking and polarity. This supports

307   that there is a common role for these proteins and their auxin-mediated phosphorylation in auxin

308   feedback on PIN-dependent auxin transport.

309

310   **Auxin-mediated Myosin XI phosphorylation in PIN3 repolarization during shoot gravitropic**

311   **bending termination**

312   Next, we tested the relevance of Myosin XI and its auxin-mediated phosphorylation in different

313   developmental contexts. During shoot gravitropic responses, gravity initially induces relocation of

314   PIN3 to the bottom sides of endodermis cells to redirect auxin towards the lower side of the

315   hypocotyl, which leads to growth promotion and upward hypocotyl bending. Subsequently, the

316 auxin build-up at the lower side mediates a second relocation of PIN3 transporters to the inner

317 lateral sides, thus re-establishing the symmetry of auxin fluxes and terminating asymmetric growth

318 (Rakusová et al., 2016). Thus, the auxin effect on PIN3 polarity for the termination of shoot

319 gravitropic bending represents an example of auxin feedback regulation of PIN-dependent auxin

320 transport.

321   Indeed, the *myosin xik xif* mutant showed impaired polar auxin transport in hypocotyl (**Figure**

322 **S8B**) and its hypocotyls were hyperbending (**Figure 6A-C**; Okamoto et al., 2015). Steady-state

323 PIN3 polarity was not affected in *myosin xik xif* mutant hypocotyls (**Figure 6D**), neither was the

324 gravity-induced PIN3 polarization in the endodermis cells after 6 hours gravistimulation (**Figure**

325 **S9**). In contrast, the auxin-mediated re-establishment of PIN3 polarity at later stages (24 hours)

326 was defective (**Figure S9**). To directly test the auxin feedback on PIN3 polarity in hypocotyls, we

327 applied auxin exogenously, which induces a similar PIN3 repolarization to inner side of

328 endodermal cells as observed at later stage of gravitropic response (Rakusová et al., 2016). Indeed,

329 we observed normal auxin-induced PIN3 repolarization in WT hypocotyls, but not in *myosin xik*

330 *xif* mutant hypocotyls (**Figure 6D; Figure S8A**). Thus, Myosin XI function is required,

331 specifically, for the auxin-mediated PIN3 repolarization and for the gravitropic bending

332 termination in hypocotyls.

333   We also tested whether the auxin-regulated Myosin XI phospho-sites is essential for PIN3

334 polarization. Gravity-induced PIN3 polarization was normal in both phospho-deficient (XIF^{S1256A};

335 XIK^{S1234A}) and non-mutated control myosin mutants (**Figure S9**). On the other hand, auxin-

336 mediated PIN3 repolarization at later stages of gravity response (**Figure S9B-C**), or after

337 exogenous auxin application (**Figure 6D; Figure S8A**), was defective in the phospho-deficient

338 mutants, whereas the non-mutated controls showed normal PIN3 repolarization. Accordingly, the

339 hypocotyls of Myosin XI phospho-deficient mutants were hyperbending **(Figure 6A-B)**.

340   These observations demonstrate that Myosin XI function and its auxin-mediated

341 phosphorylation are required for auxin-mediated PIN3 repolarization in shoot and for the resulting

342 termination of the gravitropic bending.

343

344 **Auxin-mediated Myosin XI phosphorylation in auxin canalization-mediated vasculature**

345 **formation and regeneration**

346 The classical auxin canalization hypothesis proposes auxin feedback regulation of directional

347 auxin transport as the key part underlying self-organizing aspects of plant development, such as

348 vasculature formation during spontaneously arising leaf venation patterns (Scarpella et al., 2006)

349 and flexible regeneration of vasculature around wounding sites (Sauer et al., 2006; Mazur et al.,

350 2016, 2020a, b).

351 We first analyzed cotyledon venation patterns in *myosin xik xif* mutant seedlings. As compared

352 to WT leaves, *myosin xik xif* mutants showed typically fewer loops (**Figure S8E**). We also

353 analyzed seedlings overexpressing non-mutated and phospho-deficient versions of MyosinXI

354 proteins. Cotyledons of lines expressing the *XIK^{WT}* and *XIF^{WT}* constructs did not show any

355 pronounced defects in the number of loops **(Figure S8E)**. On the other hand, seedlings expressing

356 phospho-deficient constructs (*XIK^{S1234A}* and *XIF^{S1256A}*) had a higher occurrence of fewer loops

357 **(Figure S8E)**. Thus, mutants defective either in Myosin XI function or in their auxin-mediated

358 phosphorylation show mild defects in cotyledon venation.

359 Next, we analyzed vasculature regeneration in stems after wounding. As visualized by

360 toluidine blue staining, within 7 days after wounding the vasculature fully developed in WT stems

361 and reconnected around the interruption while, in *myosin xik xif* mutant stems, the newly formed

362 vasculature was partially connected **(Figure 7A)**. We also analyzed the regeneration in phospho-

363 deficient Myosin XI transgenic plants (WT background)**(Figure 7B)**. The Myosing XI (*XIK^{WT}* and

364 *XIF^{WT}*) stems showed partial regeneration around the wound, but the phospho-deficient Myosin

365 XI stems (*XIK^{S1234A}* and *XIF^{S1256A}*) did not regenerate at all **(Figure 7B)**. Thus, mutants defective

366 either in Myosin XI function or in their auxin-mediated phosphorylation show defects in

367 vasculature regeneration around the wound.

368 The most direct manifestation of auxin-induced canalization processes, is the formation of a

369 auxin-transporting channels followed by vasculature differentiation starting at local, exogenous

370 auxin source (Mazur et al., 2016, 2020a, b). In WT stems a distinct, new vasculature strand

371 connecting the external IAA drop to the existing vasculature was formed; however, in *myosin xik*

372 *xif* mutant stems, no such formation of well defined vasculature was observed **(Figure 7C)**. Similar,

373 auxin application induced new vasculature formation in *XIF^{WT}* and *XIK^{WT}* stems , but not in

374 phospho-deficient Myosin XI mutants stems **(Figure 7C)**.

375 These results show that Myosin XI proteins and their auxin-mediated phosphorylation are

376 important for the auxin canalization-mediated vasculature formation; to a limited extent during

377   leaf venation but indispensable for the vasculature regeneration around a wound as well as for the

378   *de novo* vascular strands formation from the external auxin source. This collectively shows that

379   auxin-mediated myosin XI phosphorylation, which at the cellular level mediates auxin regulation

380   of PIN trafficking and polarity, is required for developmental processes that depend on coordinated,

381   auxin-regulated polarization of PIN-dependent auxin transport.

382

Discussion

384   Auxin, a crucial regulator of plant development, is known to trigger well-characterized nuclear

385   signaling to mediate transcriptional reprogramming, nonetheless the existence of rapid, non-

386   transcriptional cellular auxin effects has been discussed for decades (Kubeš and Napier, 2019).

387   Here, we established a fast phospho-proteomics approach, identify a thus far unknown rapid

388   phosphorylation response, and characterize novel targets of this rapid auxin signaling pathway.

389   Among the identified candidates that were phosphorylated within few minutes in response to auxin,

390   we characterized in depth Myosin XI proteins and the MadB2 Myosin binding protein. This

391   analysis identified their auxin-mediated phosphorylation as an essential part of the feedback

392   mechanism, by which auxin regulates its directional transport for the self-organizing aspects of

393   plant development.

394

Auxin mediates rapid protein phosphorylation by distinct signaling pathways

396   Protein phosphorylation and de-phosphorylation are prominent post-translational modification to

397   control protein functions and it is among the most common downstream events in many signaling

398   pathways. Therefore, in order to identify new players of the rapid auxin responses, we optimized

399   a phospho-proteomics protocol and designed treatment conditions in Arabidopsis seedling root

400   tips, allowing identification of proteins phosphorylated within 2 minutes of auxin treatment with

401   a high coverage. By using the available tools, such as the auxin antagonist specific for the

402   TIR1/AFB receptors, PEO-IAA and the engineered receptor-ligand pair cvxIAA/*ccvTIR1*, we

403   were able to distinguish auxin-induced modifications, which are dependent and independent of the

404   canonical TIR1/AFB1 signaling.

405   To our knowledge, this rapid phosphorylation response is among the fastest responses to

406   auxin reported to date. The set of proteins that is targeted by rapid auxin-dependent

407   phosphorylation is distinct from those targeted by transcriptional control (**Figure 1D**), and thus

408 represents a functionally unique aspect of auxin activity. The identified proteins targeted by this

409 rapid response are diverse in nature and function, and provide a rich source of hypotheses on

410 mechanisms mediating ultrafast, non-transcriptional auxin responses. They for example include

411 chromatin and transcriptional regulators, mediators of membrane trafficking, regulators of RNA

412 splicing and -suppression and various groups of enzymes. It is likely that these phosphorylation

413 events have a functional impact on many of these pathways. Given that the response is, at least in

414 part, independent of the TIR1 receptor, there is a potential for this response to occur in species that

415 do not have a TIR1 orthologue, such as the *Charophyceae* algae (Mutte et al., 2018). Key future

416 questions will therefore be, what receptor and downstream components mediate this ultrafast, non-

417 transcriptional auxin response, and how universal it is in the plant kingdom.

418

419 **Auxin regulates PIN trafficking and polarity via phosphorylation of myosin complex**

420 Myosin XIK and its interactor myosin-binding protein MadB2 were identified among the

421 confirmed candidates identified as being rapidly phosphorylated by TIR1-independent auxin

422 signaling. Given the concomitant auxin regulation of these group of functionally related proteins

423 and the potential role of myosin in cellular processes related to trafficking and polarity, we focused

424 on these candidates as potential new components of auxin feedback on its own polar, intercellular

425 transport, which is the key prerequisite of so-called auxin canalization (Sachs, 1981).

426 The auxin canalization hypothesis provides a mechanistic framework for flexible, self-

427 organizing plant developmental processes such as post-embryonic organogenesis, shoot branching,

428 leaf venation and vascular tissue regeneration. A key condition for canalization is the feedback

429 regulation of auxin transport, as manifested at a cellular level by the auxin effect on the polar,

430 subcellular localization of PIN auxin transporters. Constitutive PIN trafficking and clathrin-

431 mediated endocytosis represent key cellular components of this feedback regulation of PIN

432 polarity (Paciorek et al., 2005; Robert et al., 2010; Mazur 2020a; Zhang et al., 2020).

433 Our analysis revealed that the Myosin XI proteins are required for auxin-regulated PIN

434 trafficking and PIN polarity rearrangement in different developmental contexts. This is

435 demonstrated by strong defects in the corresponding loss-of-function mutants, where auxin is

436 largely unable to affect PIN subcellular trafficking or mediate PIN repolarization. Notably, similar

437 defects in auxin-mediated PIN trafficking and polarization were also observed in the phospho-

438 deficient Myosin XI transgenic lines, in which we mutated the identified auxin-dependent

439 phospho-site. This shows that auxin-mediated phosphorylation of Myosin XI proteins is crucial
440 for auxin-mediated PIN trafficking and polarity regulation.

441   The identification of a large number of myosin interacting proteins indicates there is a
442 series of specific interactions that allow myosin motors to operate on various cargoes (Peremyslov
443 et al., 2013; Kurth et al., 2017) that likely also include PIN proteins, which traffic along the actin
444 cytoskeleton (Geldner et al., 2001). Our genetic analysis demonstrates that the MadB2 myosin
445 binding protein family contributes to PIN trafficking and polarity regulation in roots. The most
446 likely scenario is that PIN proteins are cargoes of vesicles that are decorated by the MadB2 family
447 proteins, which bind to the Myosin XI proteins forming a transport network (Peremyslov et al.,
448 2013; Kurth et al., 2017). By this mechanism, PIN proteins can be transported though the
449 trafficking pathway to specific, polar destinations. Notably, auxin-mediated phosphorylation of
450 these components provides a means how auxin itself can influence this process in different
451 developmental contexts. The topics of future investigations include how the myosin binding
452 proteins convey specificity for different cargoes, how myosin tail-binding proteins are employed
453 by myosins to carry out their trafficking function and not least, how the auxin-mediated
454 phosphorylation influences the whole system to aid the required PIN polarity re-arrangement to
455 mediate redirection of auxin fluxes in different developmental processes.

456

457 **Auxin feedback on directional auxin transport in plant development**

458 With identification of Myosin XI and corresponding myosin-binding proteins, we obtained
459 molecular components of the feedback between auxin signaling and polarity re-arrangements of
460 PIN auxin transport components. This provides a genetic means to test the auxin canalization
461 hypothesis, its cellular requirements and developmental roles.

462   Firstly, the analysis of *myosin xik xif* and *madb 4KO* mutants confirmed the previously
463 proposed link between auxin effect on PIN trafficking and auxin effect on PIN polarity (Sauer et
464 al., 2006; Wabnik et al., 2010, 2011; Mazur 2020a; Zhang et al., 2020) because these mutants are
465 defective in both processes and their auxin regulation. Moreover, they also allowed to link auxin
466 effect on PIN polarity, typically visualized in roots, to similar auxin-mediated PIN rearrangements
467 in other developmental contexts, mainly those involving flexible formation of auxin channels
468 determining position of new vasculature, such as vasculature regeneration after wounding in stems.
469 Additionally, our observations confirmed that the Myosin XI-based mechanism also operates in

470 other developmental processes, which do not involve auxin channel formation, but where auxin
471 effect on PIN polarity has been observed, such as PIN3 polarization for gravitropic bending
472 termination in shoots. Hence, our findings provide mechanistic and molecular support for the auxin
473 canalization hypothesis and show that the myosin transport network and its auxin regulation play
474 an essential role in many developmental processes involving auxin canalization or auxin effect on
475 its transport directionality.

476 In conclusion, this study demonstrates that Myosin XI and MadB2 myosin binding proteins,
477 as part of the myosin transport network, are required for auxin feedback on PIN polarity, more
478 specifically for auxin effect on PIN trafficking and polarity re-arrangements. Furthermore, we also
479 uncover that auxin-mediated phosphorylation of these myosins is required and sufficient for their
480 function in PIN trafficking and polarity regulation. Our work provides first mechanistic insights
481 into feedback regulation of auxin transport and reveals its crucial role in many self-organizing
482 developmental processes involving auxin canalization.

483

Acknowledgments

491

Author Contributions

493 H. H. and J. F. designed research. H. H. performed most of the experiments. I. V. synthesized the
494 Myosin XIK and XIF GTD sequences and performed the Western blot assays. M. R. and D. W.
495 optimized, performed and analyzed the phosphoproteomics experiments. J. H. carried out the auxin
496 transport assay. K. Ö. set up the PhosTag method. E. M. and N. R. performed the regeneration
497 assays. H. H., I.V. and J. F. wrote the manuscript with input from all other authors.

498

Declaration of Interests

500 The authors declare no competing interests.

References

Abel, S., and Theologis, A. (1996). Early genes and auxin action. Plant Physiol. *111*, 9

Abas, L., Benjamins, R., Malenica, N., Paciorek, T., Wišniewska, J., Moulinier–Anzola, J. C., Sieberer, T., Friml, J. and Luschnig, C. (2006). Intracellular trafficking and proteolysis of the Arabidopsis auxin-efflux facilitator PIN2 are involved in root gravitropism. Nat. Cell Biol. *8*, 249-256

Abu-Abied, M., Belausov, E., Hagay, S., Peremyslov, V., Dolja, V. and Sadot, E. (2018). Myosin XI-K is involved in root organogenesis, polar auxin transport, and cell division. J. Exp. Bot. *69*, 2869-2881

Adamowski, M., and Friml, J. (2015). PIN-dependent auxin transport: action, regulation and evolution. Plant Cell *27*, 20-32Avisar D., Prokhnevsky, A. I., Makarova, K. S., Koonin, E. V. and Dolja, V. V. (2008) Myosin XI-K is required for rapid trafficking of golgi stacks, peroxisomes, and mithochondria in leaf cells of *Nicotiana benthamiana*. Plant Physiol. *146*: 1098-108

Avisar, D., Abu-Abied, M., Belausov, E., Sadot, E., Hawes, C. and Sparkes, I.A. (2009). A comparative study of the involvement of 17 *Arabidopsis* myosin family members on the motility of Golgi and other organelles. Plant Physiol. *150*, 700-709

Barbosa, I.C.R., Hammes, U.Z. and Schwechheimer, C. (2018). Activation and polarity control of PIN-FORMED auxin transporters by phosphorylation. Trends in Plant Sci. *23*, 523-538

Bargmann, OR B., Vanneste, S., Krouk, G., Nawy,T., Efroni, I., Shani E., Choe, G., Friml, J., Bergmann C D., Estelle, M. and Birnbaum, D K. (2013) A map of cell type-specific auxin response. Mol. Syst. Biol. 9: 688

Benková, E., Michniewicz, M., Sauer, M., Teichmann, T., Seifertová, D., Jürgens, G. and Friml, J. (2003). Local, efflux-dependent auxin gradients as a common module for plant organ formation. Cell *115*, 591-602

Bennett, T., Hines, G. and Leyser, O. (2014). Canalization: what the flux? Trends in Gen. *30*, 41-48

Bhatia, N., Bozorg, B., Larsson, A., Ohno, C., Jönsson, H. and Heisler, M. G. (2016). Auxin acts through MONOPTEROS to regulate plant cell polarity and pattern phyllotaxis. Curr. Biol. *26*, 3202-3208

Cao, M., Chen, R., Li, P., Yu, Y., Zheng, R., Ge, D., Zheng, W., Wang, X., Gu, Y., Gelova, Z., Friml, J., Zhang, H., Liu, R., He, J. and Xu, T. (2019). TMK1-mediated auxin signalling regulates differential growth of the apical hook. Nature *568*, 240-243

Dhonukshe, P., Aniento, F., Hwang, I., Robinson, D. G., Mravec, J., Stierhof, Y. D. and Friml, J. (2007). Clathrin-mediated constitutive endocytosis of PIN auxin efflux carriers in *Arabidopsis*. Curr. Biol. *17*, 520-527

Dindas, J., Scherzer, S., Roelfsema, M.R.G., von Meyer, K., Muller, H.M., Al-Rascheid, K.A.S., Palme, K., Dietrich, P., Becker, D., Bennett, M.J. and Hedrich, R. (2018). AUX1-mediated root hair auxin influx governs SCF$^{TIR1/AFB}$-type Ca^{2+} signaling. Nat. Comm. *9*, 1174

Fendrych, M., Akhmanova, M., Merrin, J., Glanc, M., Hagihara, S., Takahashi, K. and Friml, J. (2018). Rapid and reversible root growth inhibition by TIR1 auxin signaling. Nat. Plants *4*, 453-459

Gallei, M., Luschnig, C. and Friml, J. (2020). Auxin signaling in growth: Schrödinger's cat out of the bag. Curr. Opin. Plant Biol. *53*, 43-49

Geldner, N., Friml, J., Stierhof, Y. D., Jürgens, G. and Palme, K. (2001). Auxin transport inhibitors block PIN1 cycling and vesicle trafficking. Nature *413*, 425

Glanc, M., Fendrych, M. and Friml, J. (2018). Mechanistic framework for cell-intrinsic re-establishment of PIN2 polarity after cell division. Nat. Plants *4*, 1082-1088

Govindaraju, P., Verna, C., Zhu, T. and Scarpella, E. (2020). Vein patterning by tissue-specific auxin transport. Development *147*, dev187666

Hajný, J., Prát, T., Rydza, N., Rodriguez, L., Tan, S., Verstraeten, I., Domjan, D., Mazur, E., Smakowska-Luzan, E., Smet, W., Mor, E., Nolf, J., Yang, B.J., Grunewald, W., Molnár, G., Belkhadir, Y., De Rybel, B. and Friml, J. (2020). Receptor kinase module targets PIN-dependent auxin transport during canalization. Science *370*, 550-557

542 Han, H., Rakusova, H., Verstraeten, I., Zhang, Y. and Friml, J. (2020). SCF^{TIR1/AFB} auxin signaling for bending termination during
543 shoot gravitropism. Plant Physiol. *183*, 37-40

544 Haraguchi, T., Ito, K., Duan, Z., Rula, S., Takahashi, K., Shibuya, Y., Hagino, N., Miyatake, Y., Nakano, A., Tominaga, M. (2018).
545 Functional diversity of class XI Myosins in *Arabidopsis thaliana*. Plant Cell Physiol. 29: 2268-2277Hayashi, K.I., Tan, X., Zheng,
546 N., Hatate, T., Kimura, Y., Kepinski, S. and Nozaki, H. (2008). Small-molecule agonists and antagonists of F-box protein-substrate
547 interactions in auxin perception and signaling. Proc. Natl. Acad. Sci. USA *105*, 5632-5637

548 Heisler, M. G., Ohno, C., Das, P., Sieber, P., Reddy, G. V., Long, J. A. and Meyerowitz, E. M. (2005). Patterns of auxin transport
549 and gene expression during primordium development revealed by live imaging of the Arabidopsis inflorescence meristem. Curr.
550 Biol. *15*, 1899-1911

551 Hooper, C. M., Castleden, I. R., Tanz, S. K., Aryamanesh, N. and Millar, A. H. (2017). SUBA4: the interactive data analysis centre
552 for Arabidopsis subcellular protein locations. Nucleic Acids Res. *45*, D1064-D1074

553 Humphrey, S. J., Azimifar, S. B. and Mann, M. (2015). High-throughput phosphoproteomics reveals *in vivo* insulin signaling
554 dynamics. Nat. Biotechnol. *33*, 990-995.

555 Jásik, J., Bokor, B., Stuchlík, S., Mičieta, K., Mičieta, K., Schmelzer, E. (2016). Effects of auxin on PIN-FORMED2 (PIN2)
556 dynamics are not mediated by inhibiting PIN2 endocytosis. Plant Physiol. *172*, 1019-1031

557 Jelínková, A., Malínská, K., Simon, S., Kleine-Vehn, J., Parezová, M., Pejchar, P., Kubes, M., Martinec, J., Friml, J., Zazímalová,
558 E. and Petrásek J. (2010). Probing plant membranes with FM dyes: tracking, dragging or blocking? Plant J. *61*, 883-892

559 Kieffer, M., Neve, J. and Kepinski, S. (2010). Defining auxin response contexts in plant development. Curr. Opin. Plant Biol. *13*,
560 12-20

561 Kleine-Vehn, J., Leitner, J., Zwiewka, M., Sauer, M., Abas, L., Luschnig, C. and Friml, J. (2008a). Differential degradation of
562 PIN2 auxin efflux carrier by retromer-dependent vacuolar targeting. Proc. Natl. Acad. Sci. USA *105*, 17812-17817

563 Kleine-Vehn, J., Langowski, L., Wisniewska, J., Dhonukshe, P., Brewer, P.B., Friml J. (2008b). Cellular and molecular
564 requirements for polar targeting and transcytosis in plants. Mol. Plant 1, 1056-1066

565 Koonin, E. V. and Dolja, V. V. (2017). Myosin-driven transport network in plants. Proc. Natl. Acad. Sci. USA *114*, E1385-E1394

566 Kubeš, M. and Napier, R. (2019). Non-canonical auxin signalling: fast and curious. J. Exp. Bot. *70*, 2609

567 Kurth, E. G., Peremyslov, V. V., Turner, H. L., Makarova, K. S., Iranzo, J., Mekhedov, S. L.,

568 Lavy, M. and Estelle, M. (2016) Mechanisms of auxin signaling. Development *143*, 3226-3229

569 McClure, B. A., Hagen, G., Brown, C. S., Gee, M. A. and Guilfoyle, T. J. (1989). Transcription, organization, and sequence of an
570 auxin-regulated gene cluster in soybean. Plant Cell, *1*, 229-239

571 Lewis, D. R., Olex, A. L., Lundy, S. R., Turkett, W. H., Fetrow, J. S. and Muday, G. K. (2013). A kinetic analysis of the auxin
572 transcriptome reveals cell wall remodeling proteins that modulate lateral root development in Arabidopsis. Plant Cell *25*, 3329-
573 3346

574 Li, L., Verstraeten, I., Roosjen, M., Takahashi, K., Rodriguez, L., Merrin, J., Chen, J., Shabala, L., Smet, W., Ren, H., Vanneste,
575 S., Shabala, S., De Rybel, B., Weijers, D., Kinoshita, T., Gray, W.M. and Friml, J. (2021). Antagonistic cell surface and
576 intracellular auxin signalling regulate plasma membrane H+-fluxes for root growth. Research Square DOI: 10.21203/rs.3.rs-
577 266395/v1

578 Lin, W., Tang, W., Takahashi, K., Ren, H., Pan, S., Zheng, H., Gray, W.M., Xu, T., Kinoshita, T. and Zhenbiao, Y. (2021).
579 TMK-based cell surface auxin signaling activates cell wall acidification in Arabidopsis. Research Square DOI: 10.21203/rs.3.rs-
580 203621/v1

581 Mazur, E., Benková, E. and Friml, J. (2016). Vascular cambium regeneration and vessel formation in wounded inflorescence stems
582 of Arabidopsis. Sci. Rep. *6*, 33754

583 Mazur, E., Gallei, M., Adamowski, M., Han, H., Robert, H. S. and Friml, J. (2020a). Clathrin-mediated trafficking and PIN
584 trafficking are required for auxin canalization and vascular tissue formation in Arabidopsis. Plant Sci. *293*, 110414

585 Mazur, E., Kulik, I., Hajný, J. and Friml, J. (2020b). Auxin canalization and vascular tissue formation by TIR1/AFB-mediated
586 auxin signaling in Arabidopsis. New Phytol. *226*, 1375-1383

587 Michniewicz, M., Zago, M. K., Abas, L., Weijers, D., Schweighofer, A., Meskiene, I., Heisler, M. G., Ohno, C., Zhang, J., Huang,
588 F., Schwab, R., Weigel, D., Meyerowitz, E. M., Luschnig, C., Offringa, R., Friml, J. (2007). Antagonistic regulation of PIN
589 phosphorylation by PP2A and PINOID directs auxin flux. Cell *130*, 1044-1056

590 Morffy, N., and Strader, L. C. (2020). Old Town Roads: routes of auxin biosynthesis across kingdoms. Curr. Opin. Plant Biol. *55*,
591 21-27

592 Mutte, K. S., Kato, H., Rothfels,. C., Melkonian, M., Wong, G. K. and Weijers, D. (2018). Origin and evolution of the nuclear
593 auxin response system. Elife 7: e33399

594 Narasimhan, M., Johnson, A., Prizak, R., Kaufmann, W.A., Tan, S., Casillas-Pérez, B. and Friml, J. (2020). Elife *9*: e52067

595 Nikonorova, N., Van den Broeck, L., Zhu, S., Van De Cotte, B., Dubois, M., Gevaert, K., Inze, D. and De Smet, I. (2018). Early
596 mannitol-triggered changes in the Arabidopsis leaf (phospho) proteome reveal growth regulators. J. Exp. Bot. *69*, 4591-4607

597 Okamoto, K., Ueda, H., Shimada, T., Tamura, K., Kato, T., Tasaka, M., Morita, M. T. and Hara-Nishimura, I. (2015). Regulation
598 of organ straightening and plant posture by an actin–myosin XI cytoskeleton. Nat. Plants *1*, 15031

599 Ojangu, E. L., Ilau, B., Tanner, K., Talts, K., Ihoma, E., Dolja, V. V., Paves, H. and Truve, E. (2018). Class XI myosins contribute
600 to auxin response and senescence-induced cell death in *Arabidopsis*. Front. Plant Sci. *9*, 1570

601 Oochi, A., Hajny, J., Fukui, K., Nakao, Y., Gallei, M., Quareshy, M., Takahashi, K., Kinoshita, T., Harborough, S.R., Kepinski, S.,
602 Kasahara, H., Napier, R., Friml, J. and Hayashi, K. (2019). Pinstatic acid promotes auxin transport by inhibiting PIN internalization.
603 Plant Physiol. *180*, 1152-1165

604 Paciorek, T., Zažímalová, E., Ruthardt, N., Petrášek, J., Stierhof, Y. D., Kleine-Vehn, J., Morris, A. D., Emans, N., Jürgens, G.,
605 Geldner, N. and Friml, J. (2005). Auxin inhibits endocytosis and promotes its own efflux from cells. Nature *435*, 1251

606 Peremyslov, V. V., Prokhnevsky, A. I., Avisar, D. and Dolja, V. V. (2008). Two class XI myosins function in organelle trafficking
607 and root hair development in Arabidopsis. Plant Physiol. 146, 1109-1116

608 Peremyslov, V.V., Klocko, A. L., Fowler, J. E. and Dolja, V. V. (2012). Arabidopsis Myosin XI-K localizes to the motile
609 endomembrane vesicles associated with F-actin. Front. Plant Sci. 3: 184

610 Peremyslov, V. V., Morgun, E. A., Kurth, E. G., Makarova, K. S., Koonin, E. V. and Dolja, V. V. (2013). Identification of myosin
611 XI receptors in Arabidopsis defines a distinct class of transport vesicles. Plant Cell *25*, 3022-3038

612 Petrášek, J., Mravec, J., Bouchard, R., Blakeslee, J. J., Abas, M., Seifertová, D., Wisniewska, J., Tadele, Z., Kubes, M., Covanova,
613 M., Dhonukshe, P., Skupa, P., Benkova, E., Perry, L., Krecek, P., Lee, O.R., Fink, G.R., Geisler, M., Murphy, A.S., Luschnig, C.,
614 Zazimalova, E.and Friml, J. (2006). PIN proteins perform a rate-limiting function in cellular auxin efflux. Science *312*, 914-918

615 Prát, T., Hajný, J., Grunewald, W., Vasileva, M., Molnár, G., Tejos, R., Schmid, M, Sauer, M. and Friml, J. (2018). WRKY23 is a
616 component of the transcriptional network mediating auxin feedback on PIN polarity. PLoS Genet. *14*, e1007177

617 Prokhnevsky, A. I., Peremyslov, V. V. and Dolja, V. V. (2008). Overlapping functions of the four class XI myosins in *Arabidopsis*
618 growth, root hair elongation, and organelle motility. Proc. Natl. Acad. Sci. USA *105*, 19744-19749

619 Rakusová, H., Abbas, M., Han, H., Song, S., Robert, H. S. and Friml, J. (2016). Termination of shoot gravitropic responses by
620 auxin feedback on PIN3 polarity. Curr. Biol. 26, 3026-3032

621 Rakusová, H., Gallego-Bartolomé, J., Vanstraelen, M., Robert, H. S., Alabadí, D., Blázquez, M. A., Benkova, E. and Friml, J.
622 (2011). Polarization of PIN3-dependent auxin transport for hypocotyl gravitropic response in *Arabidopsis thaliana*. Plant J. *67*,
623 817-826

624 Rakusová, H., Han, H., Valošek, P. and Friml, J. (2019). Genetic screen for factors mediating PIN polarization in gravistimulated
625 *Arabidopsis thaliana* hypocotyls. Plant J. *98*, 1048-1059

626 Reddy, A. S. and Day, I. S. (2001). Analysis of the myosins encoded in the recently completed *Arabidopsis thaliana* genome
627 sequence. Genome Biol. *2*, research0024

628 Robert, H. S., Grones, P., Stepanova, A. N., Robles, L. M., Lokerse, A. S., Alonso, J. M., Weijers, D. and Friml, J. (2013). Local
629 auxin sources orient the apical-basal axis in Arabidopsis embryos. Curr. Biol. *23*, 2506-2512

630 Robert, S., Kleine-Vehn, J., Barbez, E., Sauer, M., Paciorek, T., Baster, P., Vanneste, S., Zhang, J., Simon, S., Covanova, M.,
631 Hayashi, K., Dhonukshe, P., Yang, Z., Bednarek, S.Y., Jones, A.M., Luschnig, C., Aniento, F. and Friml, J. (2010). ABP1 mediates
632 auxin inhibition of clathrin-dependent endocytosis in Arabidopsis. Cell *143*, 111-121

633 Robert, H. S., Park, C., Gutièrrez, C. L., Wójcikowska, B., Pěnčík, A., Novák, O., Chen, J., Grunewald, W., Dresselhaus, T., Friml,
634 J. and Laux, T. (2018). Maternal auxin supply contributes to early embryo patterning in Arabidopsis. Nat. Plants, *4*, 548-553

635 Ryan, J. M. and Nebenführ, A. (2017). Update on myosin motors: molecular mechanisms and physiological functions. Plant Physiol.
636 *176*, 119-127

637 Sachs, T. (1981). The control of the patterned differentiation of vascular tissues. Adv. Bot. Res. *9*, 151–162

638 Salanenka, Y., Verstraeten, I., Löfke, C., Tabata, K., Naramoto, S., Glanc, M. and Friml, J. (2018). Gibberellin DELLA signaling
639 targets the retromer complex to redirect protein trafficking to the plasma membrane. Proc. Natl. Acad. Sci. USA, *115*, 3716-3721

640 Salehin, M., Bagchi, R. and Estelle, M. (2015). SCF$^{TIR1/AFB}$-based auxin perception: mechanism and role in plant growth and
641 development. Plant Cell *27*, 9-19

642 Sauer, M., Balla, J., Luschnig, C., Wiśniewska, J., Reinöhl, V., Friml, J. and Benková, E. (2006). Canalization of auxin flow by
643 Aux/IAA-ARF-dependent feedback regulation of PIN polarity. Genes Dev. *20*, 2902-2911

644 Scarpella, E., Marcos, D., Friml, J. and Berleth, T. (2006). Control of leaf vascular patterning by polar auxin transport. Genes Dev.
645 *20*, 1015-1027

646 Stecker, K.E., Minkoff, B.B. and Sussman, M. R. (2014). Phosphoproteomic analyses reveal early signaling events in the osmotic
647 stress response. Plant Physiol. *165*, 1171-1187

648 Steinman, M.Q. and Trainor, B.C. (2010). Rapid Effects of Steroid Hormones on Animal Behavior. Nature Education Knowledge
649 *3*, 1

650 Talts, K., Ilau, B., Ojangu, E. L., Tanner, K., Peremyslov, V. V., Dolja, V. V., Truve, E. and Paves, H. (2016). Arabidopsis myosins
651 XI1, XI2, and XIK are crucial for gravity-induced bending of inflorescence stems. Front. Plant Sci. *7*, 1932

652 Tan, S., Luschnig, C., Friml, J. (2021) Pho-view of Auxin: Reversible protein phosphorylation in auxin biosynthesis, transport and
653 signaling. Mol. Plant *14*, 151-165

654 Tan, S., Zhang, X., Kong, W., Yang, X. L., Molnár, G., Vondráková, Z., Filepova, R., Petrasek, J., Friml, J. and Xue, H.W. (2020).
655 The lipid code-dependent phosphoswitch PDK1–D6PK activates PIN-mediated auxin efflux in Arabidopsis. Nat. Plants *6*, 556-
656 569

657 Uchida, N., Takahashi, K., Iwasaki, R., Yamada, R., Yoshimura, M., Endo, T.A., Kimura, S., Zhang, H., Nomoto, M., Tada, Y.,
658 Kinoshita, T., Itami, K., Hagihara, S. and Torii, K.U. (2018). Chemical hijacking of auxin signaling with an engineered auxin-TIR1
659 pair. Nat. Chem. Biol. *14*, 299-305

660 Vanneste, S. and Friml, J. (2009). Auxin: a trigger for change in plant development. Cell *136*, 1005-1016

661 Vu, L. D., Stes, E., Van Bel, M., Nelissen, H., Maddelein, D., Inzé, D. and De Smet, I. (2016). Up-to-date workflow for plant
662 (phospho) proteomics identifies differential drought-responsive phosphorylation events in maize leaves. J. of Proteome Res. *15*,
663 4304-4317

664 Wabnik, K., Govaerts, W., Friml, J. and Kleine-Vehn, J. (2011). Feedback models for polarized auxin transport: an emerging trend.
665 Mol. Syst. Biol. *7*, 2352-2359

666 Wabnik, K., Kleine‑Vehn, J., Balla, J., Sauer, M., Naramoto, S., Reinöhl, V., Merks, R.M.H., Govaerts, W. and Friml, J. (2010).

667 Emergence of tissue polarization from synergy of intracellular and extracellular auxin signaling. Mol. Syst. Biol. *6*, 447

668 Weijers, D. and Wagner, D. (2016). Transcriptional responses to the auxin hormone. Ann. Rev. Plant Biol. *67,* 539-574

669 Wendrich, J. R., Boeren, S., Möller, B. K., Weijers, D. and De Rybel, B. (2017). In vivo identification of plant protein complexes

670 using IP-MS/MS. Methods Mol. Biol. *1497*, 147-158

671 Wiśniewska, J., Xu, J., Seifertová, D., Brewer, P. B., Růžička, K., Blilou, I., Rouquie, D., Benkova, E., Scheres, B. and Friml, J.

672 (2006). Polar PIN localization directs auxin flow in plants. Science *312*, 883-883

673 Wu, L., Hu, X., Wang, S., Tian, L., Pang, Y., Han, Z., Wu, L. and Chen, Y. (2015). Quantitative analysis of changes in the

674 phosphoproteome of maize induced by the plant hormone salicylic acid. Sci. Rep. *5*, 1-16

675 Xiao, Y. and Offringa, R. (2020). PDK1 regulates auxin transport and Arabidopsis vascular development through AGC1 kinase

676 PAX. Nat. Plants *6*, 544-555

677 Xu, T., Dai, N., Chen, J., Nagawa, S., Cao, M., Li, H., Zhou, Z., Chen, Z., De Rycke, R. Rakusova, H., Wang, W., Jones, A.M.,

678 Friml, J., Patterson, S.E., Bleecker, A.B. and Yang, Z. (2014). Cell surface ABP1-TMK auxin-sensing complex activates ROP

679 GTPase signaling. Science *343*, 1025-1028

680 Žádníková, P., Petrášek, J., Marhavý, P., Raz, V., Vandenbussche, F., Ding, Z., Schwarzerová, K., Morita, M. T., Tasaka, M.,

681 Hejátko, J., Van Der Straeten, D., Friml, J. and Benková, E. (2010). Role of PIN-mediated auxin efflux in apical hook development

682 of *Arabidopsis thaliana*. Development *137*, 607-617

683 Zhang, H., Zhou, H., Berke, L., Heck, A. J., Mohammed, S., Scheres, B. and Menke, F. L. (2013). Quantitative phosphoproteomics

684 after auxin-stimulated lateral root induction identifies an SNX1 protein phosphorylation site required for growth. Mol. Cell

685 Proteomics *12*, 1158-1169

686 Zhang, J., Mazur, E., Balla, J., Gallei, M., Kalousek, P., Medveďová, Z., Li, Y., Wang, Y., Prat, T., Vasileva, M., Reinohl, V.,

687 Prochazka, S., Halouzka, R., Tarkowski, P., Luschnig, C., Brewer, P.B. and Friml, J. (2020). Strigolactones inhibit auxin feedback

688 on PIN-dependent auxin transport canalization. Nat. Commun. *11*, 1-10

689 Zhang, J., Nodzyński, T., Pěnčík, A., Rolčík, J. and Friml, J. (2010). PIN phosphorylation is sufficient to mediate PIN polarity and

690 direct auxin transport. Proc. Natl. Acad. Sci. USA *107*, 918-922

691

692 **Figures**

693 **Figure 1. Phospho-proteomic analysis reveals rapid phosphorylation in response to auxin.**
694 (A) Schematic depiction of the phospho-peptide enrichment protocol. Root tips of 5 days old Arabidopsis
695 seedlings were treated for 2 minutes and were harvested immediately. Proteins were extracted and digested
696 to peptides that were submitted to the optimized FASP-C18-Ti^{4+} phospho-peptide enrichment protocol
697 before analysis on LC-MSMS.
698 (B) ^{2}log fold changes of significantly hypo- and hyper-phosphorylated phospho-peptides (FDR ≤0.05) in
699 WT treated for 2 min with either 100 nM IAA, 1 µM cvxIAA in cTIR/*ccvTIR1* or 10 µM PEO-IAA in WT
700 compared to control treatment.
701 (C) Comparison between the 2 min 100 nM IAA phospho-proteome dataset and a previously published
702 phospho-proteome of roots stimulated with 10 µM NAA for 120 min (Zhang et al., 2013). The intersection
703 contains specific auxin-upregulated phospho-peptides such as SNX1 and AHA2, for which MS intensity in
704 the replicate samples of IAA and control treatments is depicted.
705 (D) Comparison between differentially regulated phospho-peptides (FDR ≤0.05) in the short-term 100 nM
706 IAA treatment and a published 30 min 1 µM IAA root transcriptome (Lewis et al. 2013).
707 (E) Overlap of significantly regulated phospho-peptides by 100 nM IAA, 10 µM PEO-IAA and 1 µM
708 cvxIAA treatment (FDR ≤0.05).
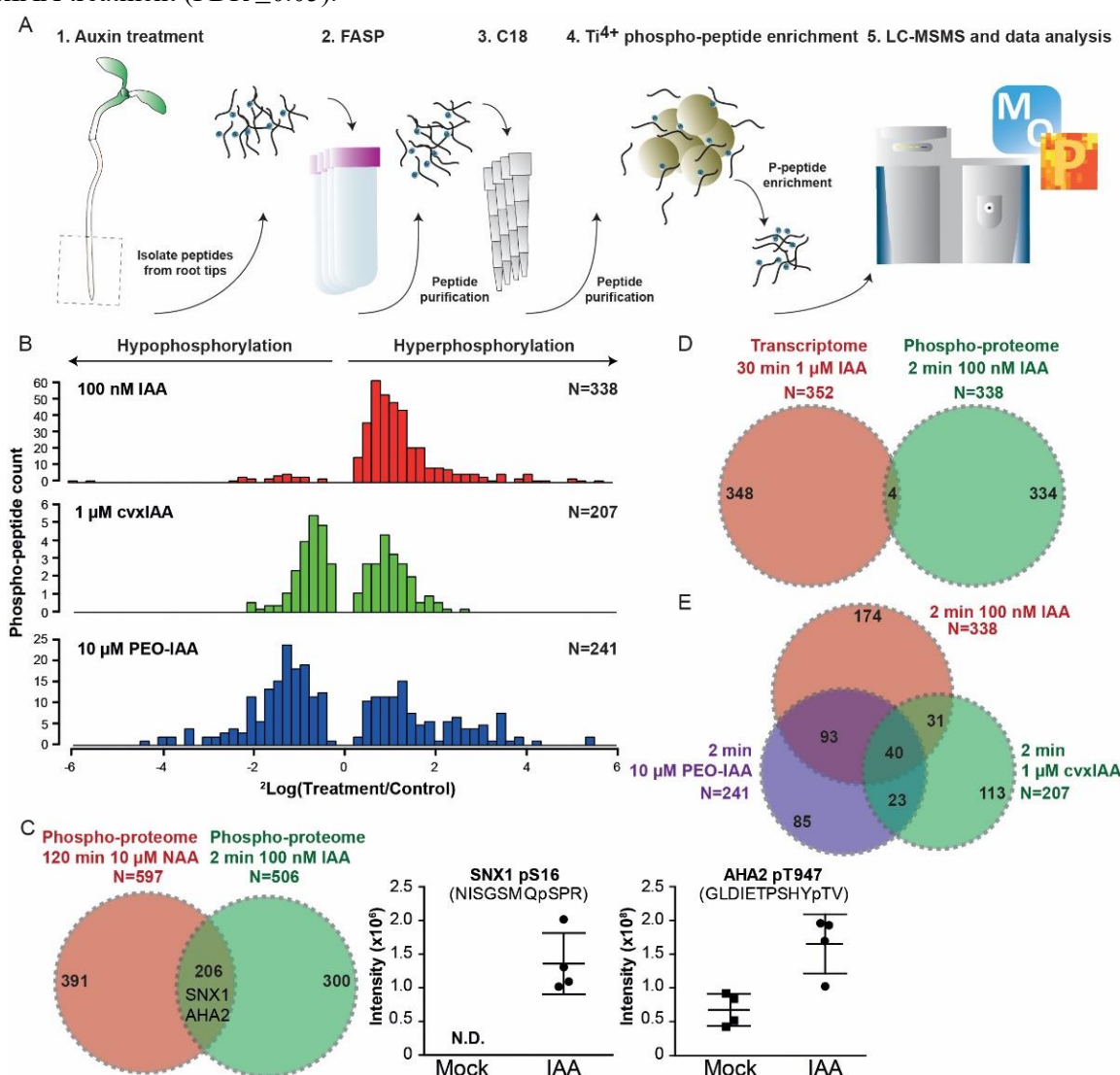
709 **Figure 2. Rapid auxin-induced phosphorylation of Myosin XI and MadB2.**
710 (A) Relative MS intensity of the auxin-induced Myosin XIK phospho-peptide (containing S1234 as the
711 significantly identified phospho-site) in 100 nM IAA, 10 µM PEO-IAA and 1 µM cvxIAA treated roots,
712 always next to the respective mock (or control line such as cTIR1 for the cxvIAA treatment in the
713 engineered *ccvTIR1* roots). In the schematic domain structure of Myosin XIK, the S1234 phospho-site
714 located in the globular tail is indicated. Experiment performed in 4 independent biological replicates,
715 represented as mean ± SD.
716 (B) Relative MS intensity of auxin-induced phospho-peptide of MadB2/PHOX2 (containing S263 as the
717 significantly identified phospho-site) in 100 nM IAA, 10 µM PEO-IAA and 1 µM cvxIAA treated roots,
718 always next to the respective mock control (or control line such as cTIR1 for the cxvIAA treatment in the
719 engineered *ccvTIR1* roots). In the schematic representation of MadB2 the S263 phospho-site is indicated.
720 Experiment performed in 4 independent biological replicates, represented as mean ± SD.
721 (C) Phosphorylation of Myosin XIK after auxin treatment visualized by Western and Phos-tag blot assays.
722 7 days old whole *35S::MyosinXIK^{WT}* seedlings were mock or 10 µM NAA treated for 30 minutes after
723 which proteins were extracted and submitted to Western and Phos-tag blot analysis. Quantification of the
724 intensities of the target proteins in the Phos-tag blot compared to normal Western, normalized to the anti-
725 actin loading control within the same sample lane, indicate a different phospho-state of the protein, which
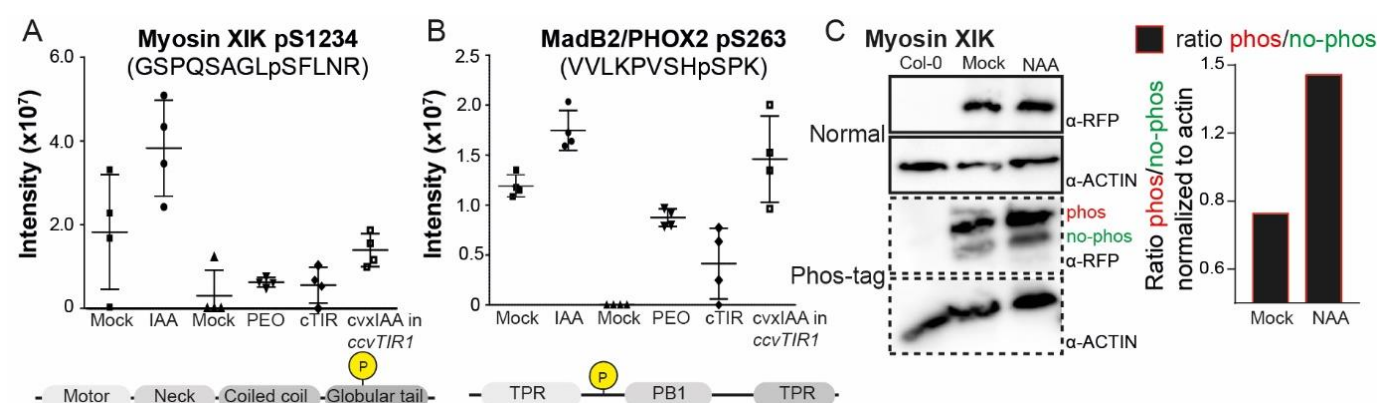726 increased in the NAA-treated samples.
727

728
729
730 **Figure 3. Myosin XI is involved in auxin-sensitive endomembrane PIN trafficking**
731 (A) Representative images demonstrating the effect of BFA treatment or the co-treatment BFA + NAA in
732 WT and *myosin xik xif* mutant roots. 3 days old seedlings were pre-treated with 10 µM NAA or DMSO
733 mock for 30 minutes and then co-treated with 50 µM BFA and 10 µM NAA for another 60 minutes followed
734 by anti-PIN1 antibody immunostaining according to Sauer et al. (2016). Scale bar = 10 µm.
735 (B) Quantification of 50 µM BFA-induced bodies in WT and *myosin xik xif* roots and co-treatment of 50
736 µM BFA with 10 µM NAA. The average number of BFA bodies was determined per root, including a
737 correction for the total number of cells evaluated per root. n > 20. Average # of BFA bodies per root ± SD
738 is represented. **** for $p \leq 0.0001$ and ns for $p > 0.05$ determined by Tukey's multiple comparison test.
739 (C) Representative confocal images of FM4-64 staining in WT and *myosin xik xif* roots. PM staining and
740 internalization of FM4-64 staining was quantified in 4 days old seedlings treated with 10 µM NAA or
741 DMSO mock for 30 minutes. Scale bar = 10 µm.
742 (D) Quantification of FM4-64 staining in WT and *myosin xik xif* roots. The CM/PM ratio was calculated
743 by dividing the intercellular signal intensity by the PM-intensity. Bars represent the mean ± SD.
744 Observations were made in more than 10 different roots and more than 20 cells per root were quantified.
745 *** for $p \leq 0.001$ and **** for $p \leq 0.0001$ determined by Tukey's multiple comparison test.
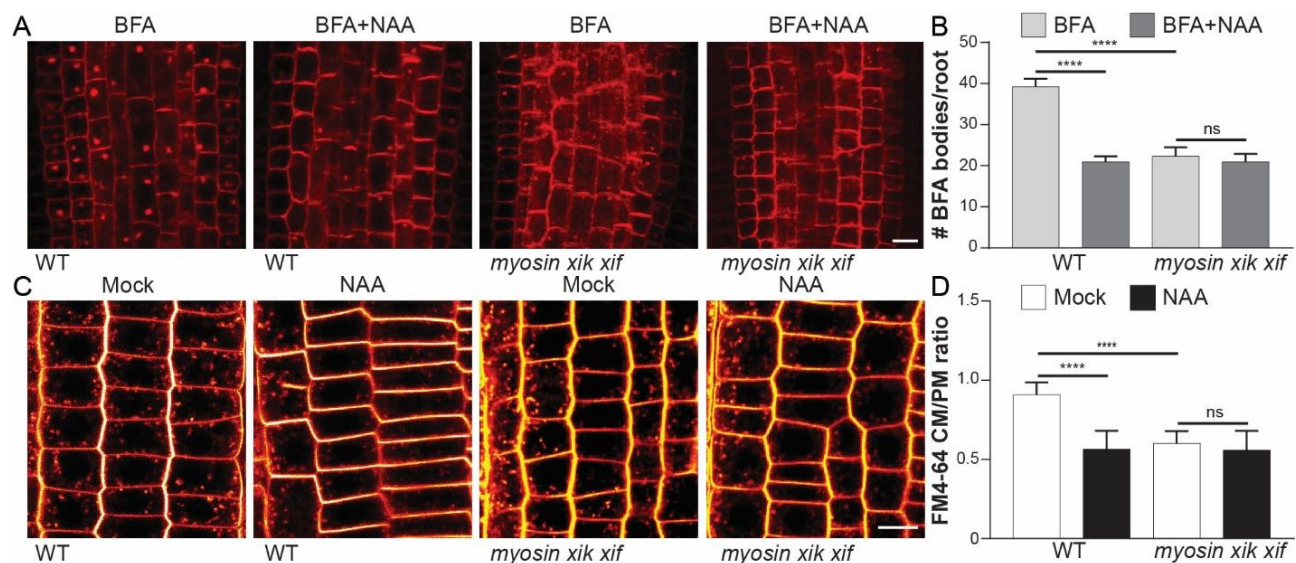746

747
748
Figure 4. Auxin-mediated Myosin XI protein phosphorylation is required for PIN trafficking.
(A) Representative set of images showing the effect of 50 µM BFA or 50 µM BFA + 10 µM NAA co-treatment in Myosin XIK^{WT} and phospho-deficient mutants (XIK^{S1234A}) in WT background. Seedlings were immunostained using anti-PIN1 antibody according to Sauer et al. (2006). Scale bar = 10 µm.
(B) Quantification of the average number of BFA bodies per root in the Myosin XI non-mutated and phospho-deficient lines in WT background. Data and error bars represent the mean ± SD. n > 15. **** p ≤ 0.0001 determined by Tukey's multiple comparison test.
(C) Representative confocal images of FM4-64 staining in *Myosin XIK^{WT}* and phospho-deficient mutants (*XIK^{S1234A}*) in WT background. CM and PM staining were observed in 4 days old seedlings treated with 10 µM NAA or DMSO mock for 30 minutes followed by a staining using 2 µM of FM4-64. Scale bar = 10 µm.
(D) Quantification of FM4-64 uptake in non-mutated and phospho-deficient Myosin XIF/XIK lines in WT background. The CM/PM ratio was calculated by dividing the internal staining intensity by the PM-intensity. Bars represent the mean ± SD of at least 40 cells in at least 10 independent roots. **** p ≤0.0001 determined by Tukey's multiple comparison test.

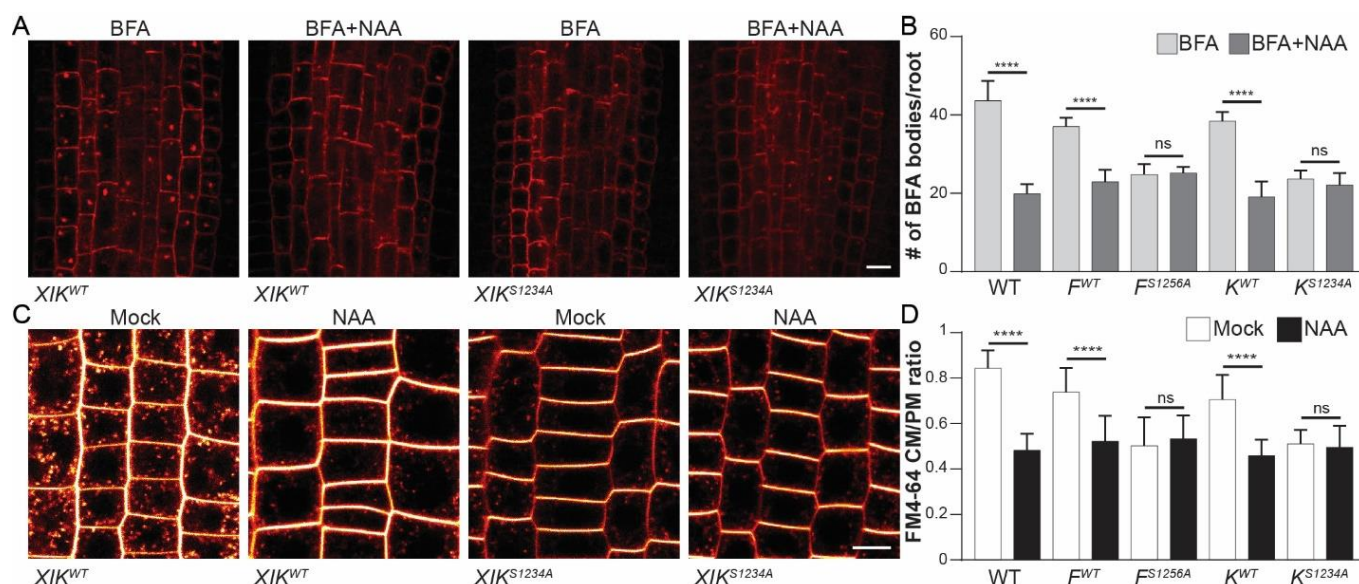764 **Figure 5. Auxin-mediated Myosin XI phosphorylation is required for PIN1 polarity regulation.**

765 (A) Representative images of DMSO mock and 10 µM NAA-induced PIN1 lateralization in WT, *myosin*

766 *xik xif* mutants and roots expressing phospho-deficient *XIK^{S1234A}*. The arrowheads indicate the predominant

767 PIN1 localization in the endodermal cells. Scale bar = 10 µm.

768 (B) Schematic representation of auxin-induced PIN1 lateralization in the endodermis of the root meristem.

769 (C) Quantification of auxin-mediated PIN1 lateralization in endodermal root cells of WT, *myosin xik xif*

770 and different lines expressing non-mutated or phospho-deficient *MyosinXIK/F* constructs (**Figure 5A** and

771 **Figure S6A**). To visualize auxin-induced lateralization, the intensity ratio of lateral to basal PIN1 signal

772 intensity was calculated per cell. Data represent mean ± SD. More than 50 cells were evaluated in at least

773 15 independent roots. **** p ≤0.0001 determined by Tukey's multiple comparison test.

774

775
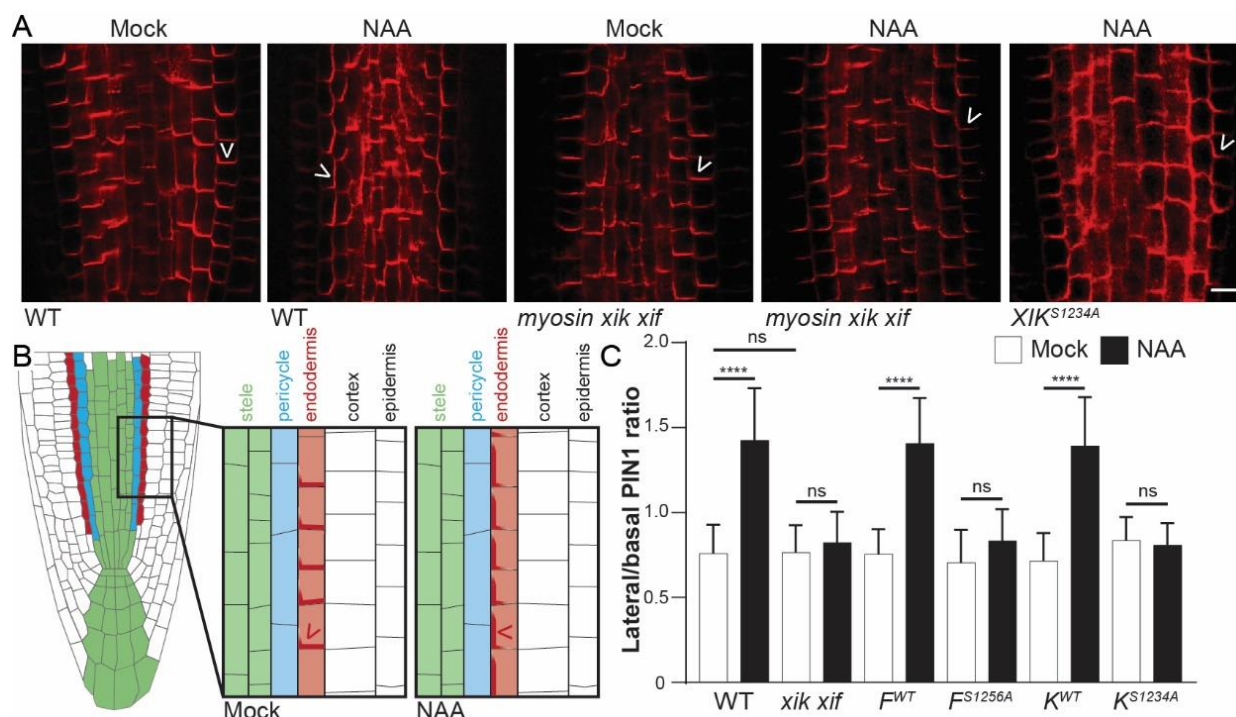
776 **Figure 6. Phosphorylation of myosin XI proteins contributes to auxin-mediated PIN3 polarity**

777 **regulation to terminate hypocotyl bending.**

778 (A) Representative seedlings showing gravity-induced hypocotyl bending. *myosin xik xif* bended stronger

779 than Col-0 WT and similarly, the phospho-deficient Myosin XIF^{S1256A} and XIK^{S1234A} were bending more

780 than their respective WT controls.

781 (B) Bending angle of hypocotyls expressing Col-0 WT, *myosin xik xif,* non-mutated and phospho-deficient

782 Myosin XIF and XIK constructs (in WT background). The bending angle was quantified in 3 days old

783 etiolated seedlings gravistimulated for 24 hours. The myosin *xik xif* mutant and the phospho-deficient

784 XIF^{S1256A} and XIK^{S1234A} showed hyperbending.

785 (C) Kinetics of the gravitropic hypocotyl bending in WT and *myosin xik xif* seedlings. More than 30

786 hypocotyls were followed over time and the average bending angle ± SD is represented. ** p ≤ 0.01, *** p

787 ≤0.001 and **** p ≤0.0001 determined by Student t-tests compared to the bending angle in WT at the same

788 timepoint.

789 (D) Representative images showing PIN3-GFP localization in WT, *myosin xik xif* mutant and hypocotyls

790 of the phospho-deficient *XIK^{S1234A}* mutant (WT background) upon mock and 10 µM NAA treatment. Scale

791 bar = 25 µm.

792 (E) Schematic depiction of auxin-induced PIN3 repolarization in the endodermis of WT etiolated
793 hypocotyls.

794 (F) Quantification of auxin-mediated PIN3 repolarization in the hypocotyl of WT, *myosin xik xif* and the
795 different *XIF^WT^/XIK^WT^*, and phospho-deficient mutants (in WT background) (**Figure 6A** and **Figure S8A**).
796 The inner/outer endodermal ratio is determined by dividing the PIN3-GFP fluorescence signal intensity
797 between inner side and outer side of hypocotyl endodermal cells. Data and error bars represent the mean ±
798 SD.
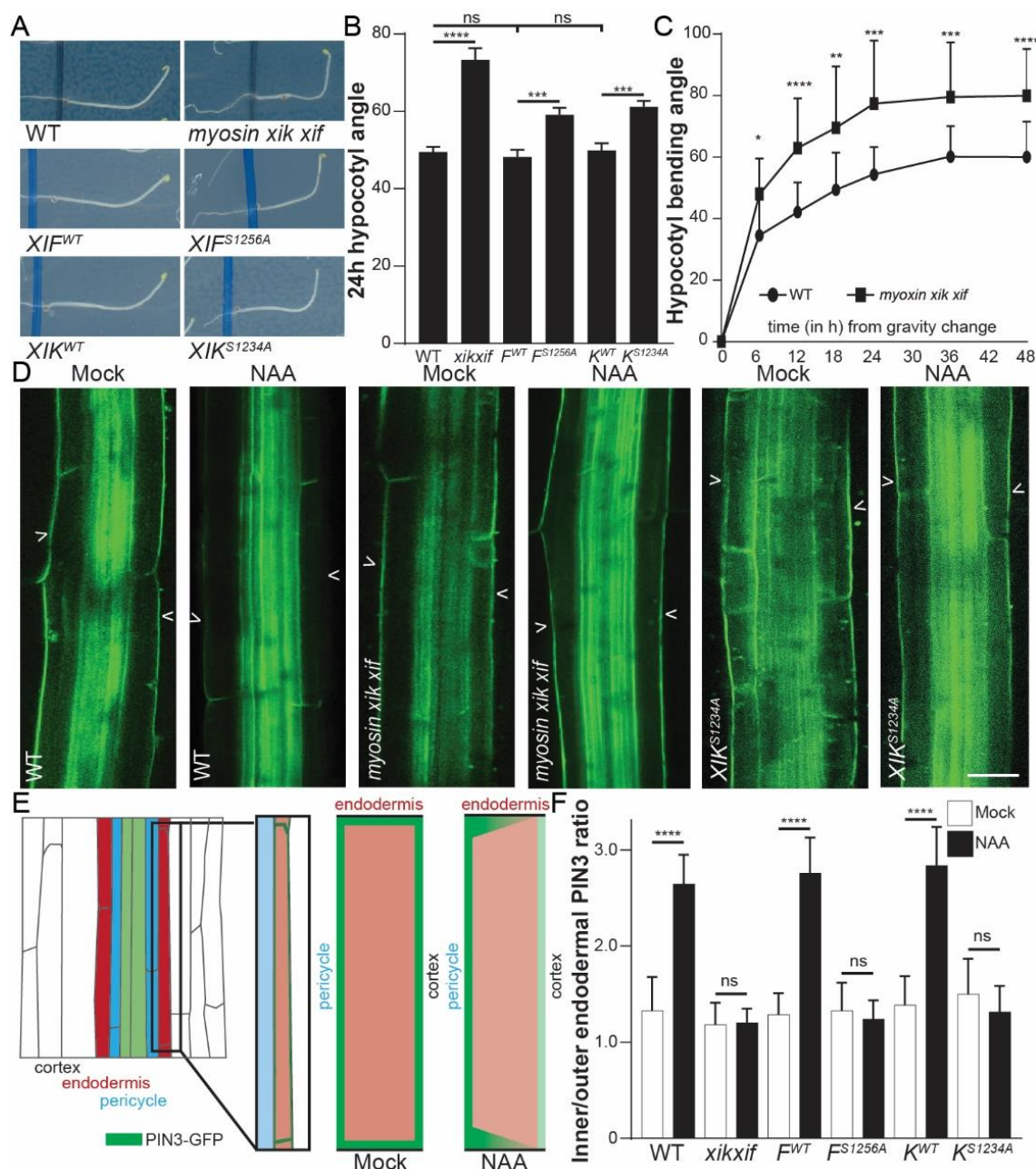
799 **Figure 7. Auxin canalization-mediated vasculature formation and regeneration depends on auxin-**
800 **mediated Myosin XI phosphorylation.**
801 (A) Vasculature regeneration in wounded *Arabidopsis thaliana* stems. The incision site is marked by a red
802 arrow. 7 days after wounding (DAW) all WT stems regenerated vasculature tissue around the wound,
803 visualized by toluidine blue staining while in the *myosin xik xif* mutants, this regeneration was defective
804 and the newly formed vasculature was incomplete. Scale bar = 100 µm.
805 (B) Representative sections and quantification of vasculature regeneration in wounded *Arabidopsis* stems
806 of *XIF^{WT}/XIK^{WT}* and the phospho-deficient mutants (WT background). Whereas the vasculature in stems
807 expressing the WT constructs (XIF^{WT} and XIK^{WT}) was regenerating, we did not observe vasculature
808 regeneration in stems expressing the phospho-deficient constructs (XIF^{S1256A} and XIK^{S1234A}). Red
809 arrowhead shows the incision site. n =20. Scale bar = 200 µm.
810 (C) Auxin-induced canalization in wounded *Arabidopsis* stems of XIF^{WT}/XIK^{WT} and the phospho-deficient
811 mutants (WT background). Exogenous IAA application (indicated by the oval shape) triggered the
812 formation of a channel (indicated by the white arrow) from this source to the existing vascular tissue
813 (visualized by toluidine blue). Channel formation was observed in stems expressing *XIF^{WT}* and *XIK^{WT}*.
814 However, regeneration failed in stems expressing the phospho-deficient constructs (*XIF^{S1256A}* and *XIK^{S1234A}*).
815 Red arrowhead shows the incision site and the white arrow indicates the newly formed channel. Scale bar
816 = 200 µm.
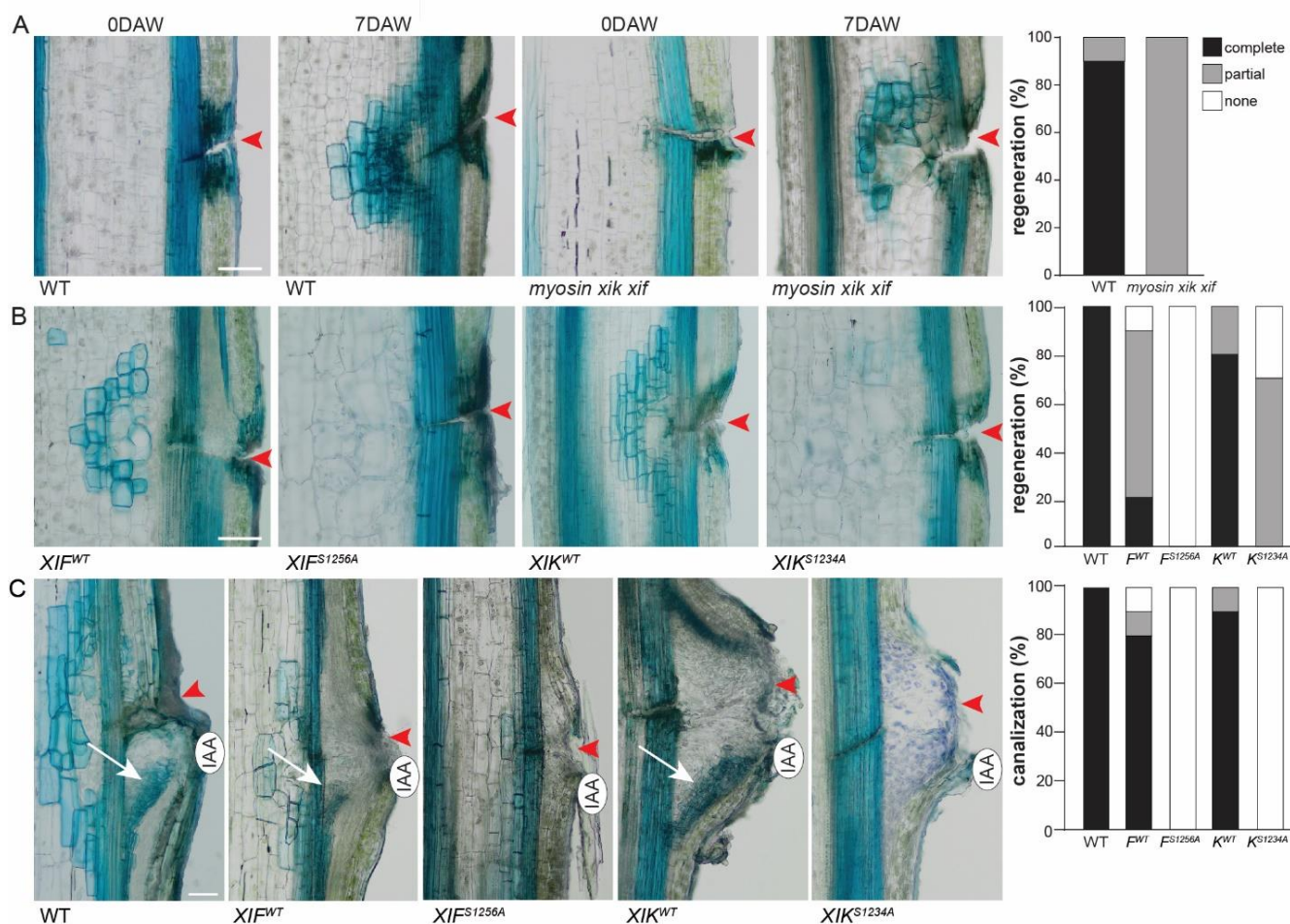
Supplemental Figures

Figure S1. Comparison of different protein precipitation and phospho-peptide enrichments strategies.
(A, B) Magnetic IMAC Ti^{4+}(Mg), MOAC TiO_2(Mg) and agarose MOAC TiO_2(TS) enrichment strategies were compared for phosphopeptide enrichment performance. IMAC outperformed the MOAC methods by identifying ~3 fold more phosphopetides. All strategies were conducted in technical triplicate.
(C) In order to analyse nucleic acid interference, to peptides digested samples were compared to 5 % protein lysate input material on a DNA agarose gel. Acetone and methanol/chloroform percipitation techniques retained nucleic acids and performed poorly for the identified number of phosphopeptides. TCA and FASP on the other hand clearly were more optimal precipitation strategies. All samples were handled in technical triplicates and phosphopeptides were enriched by the Ti^{4+}-IMAC method.
(D) Venn diagram of enriched phosphopeptides showed relatively litlle overlap between the different enrichment methods. Besides having higher numbers of phosphopeptide detection **(Figure S1B)**, this graph also indicates that Ti^{4+}-IMAC resulted in more uniquely identified phospho-sites.
(E) Motif analysis from the specific enriched peptides using the different phosphopeptide enrichment strategies. The color codes of the surrounding amino acids indicate their neutral, acidic, basic, polar or hydrophobic state. The higher presence of acidic amino acids in the TiO_2(Mg) strategie, indicates a bias of the method towards acidic peptides.
(F) The overall nature of phosphorylated amino acids followed a distribution considered normal (Wu et al. 2016) and no discernable differences were observed between the different methods.
(G) The charge state of the identified phosphopeptides (namely single, double of triple) did not differ significantly between the different enrichment methods evaluated.
(H-J) The biochemical properties of specific peptides confirmed the bias in acidic peptides for TiO_2(Mg) (lower pI in **Figure S1I**), but the hydrophobility and peptide length of the identified peptides were rather comparable (**Figure S1H-J**).
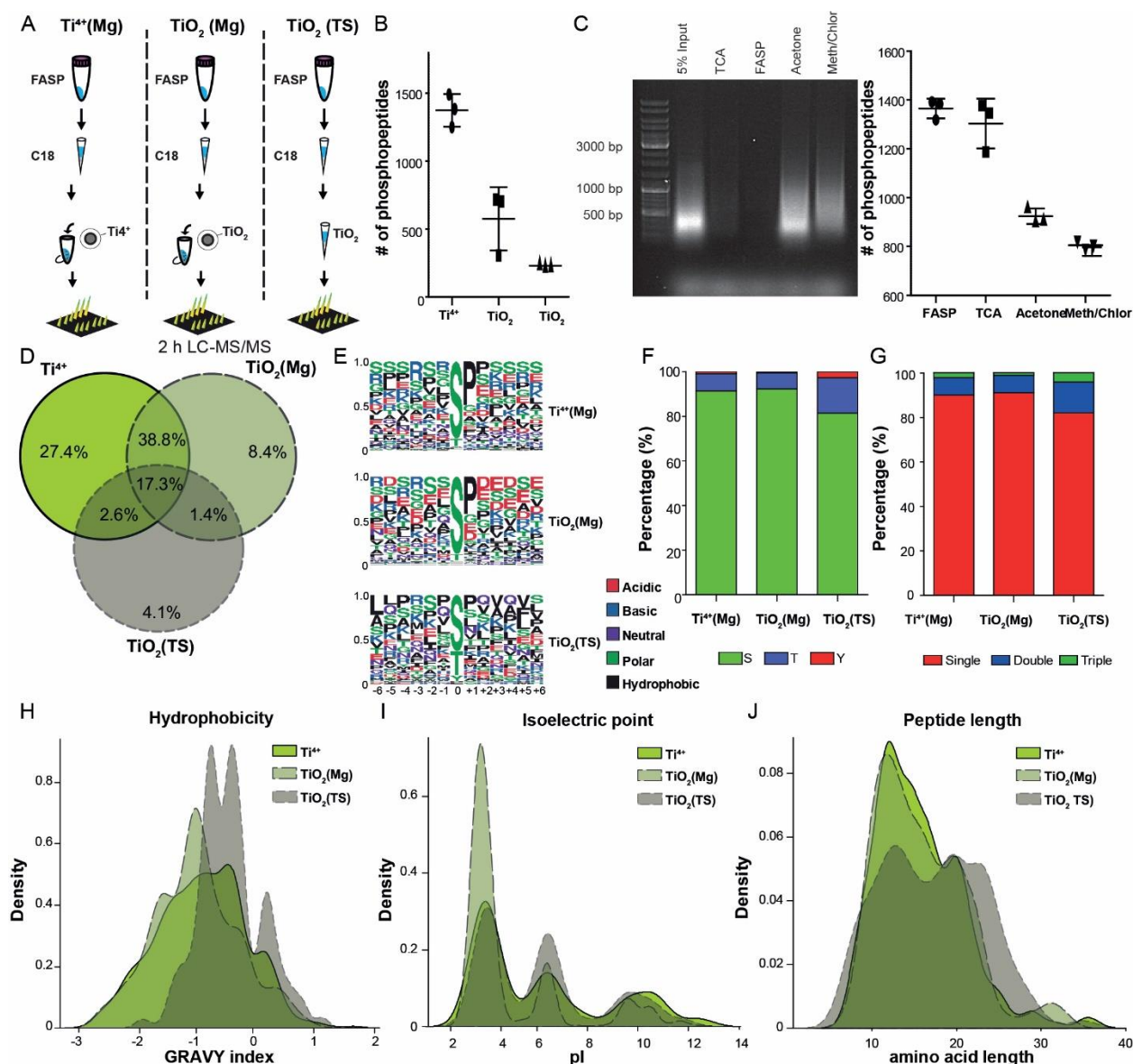
Figure S2. Analysis of phospho-peptide datasets.

(A) TIR1-independent and TIR1-dependent rapid auxin response. TIR1-independent, significantly IAA-regulated phospho-peptides, do often show an opposite effect in the PEO-IAA dataset and correspondingly lacked regulation in the cvxIAA dataset (seen by the predominantly black color).

(B) The TIR1-dependent, significantly regulated phospho-sites from the cvxIAA treatment did barely overlap with the IAA and PEO-IAA phospho-sites, visualized by the dark colors in these two datasets versus significant up- or downregulation in the cvxIAA sample.

(C) The proteins corresponding to differentially regulated phospho-peptides (FDR ≤0.05) from the 100 nM IAA dataset show a predominant localization in the nucleus, cytoplasm and at the plasma membrane.

(D) The distribution of phosphorylated amino acids did not significantly differ between IAA, PEO-IAA and cvxIAA treatment and followed the generally expected pattern: Serine(S) ~90%, Threonine(T) ~7 and Tyrosine(Y) ~1% (Wu et al. 2015).

855
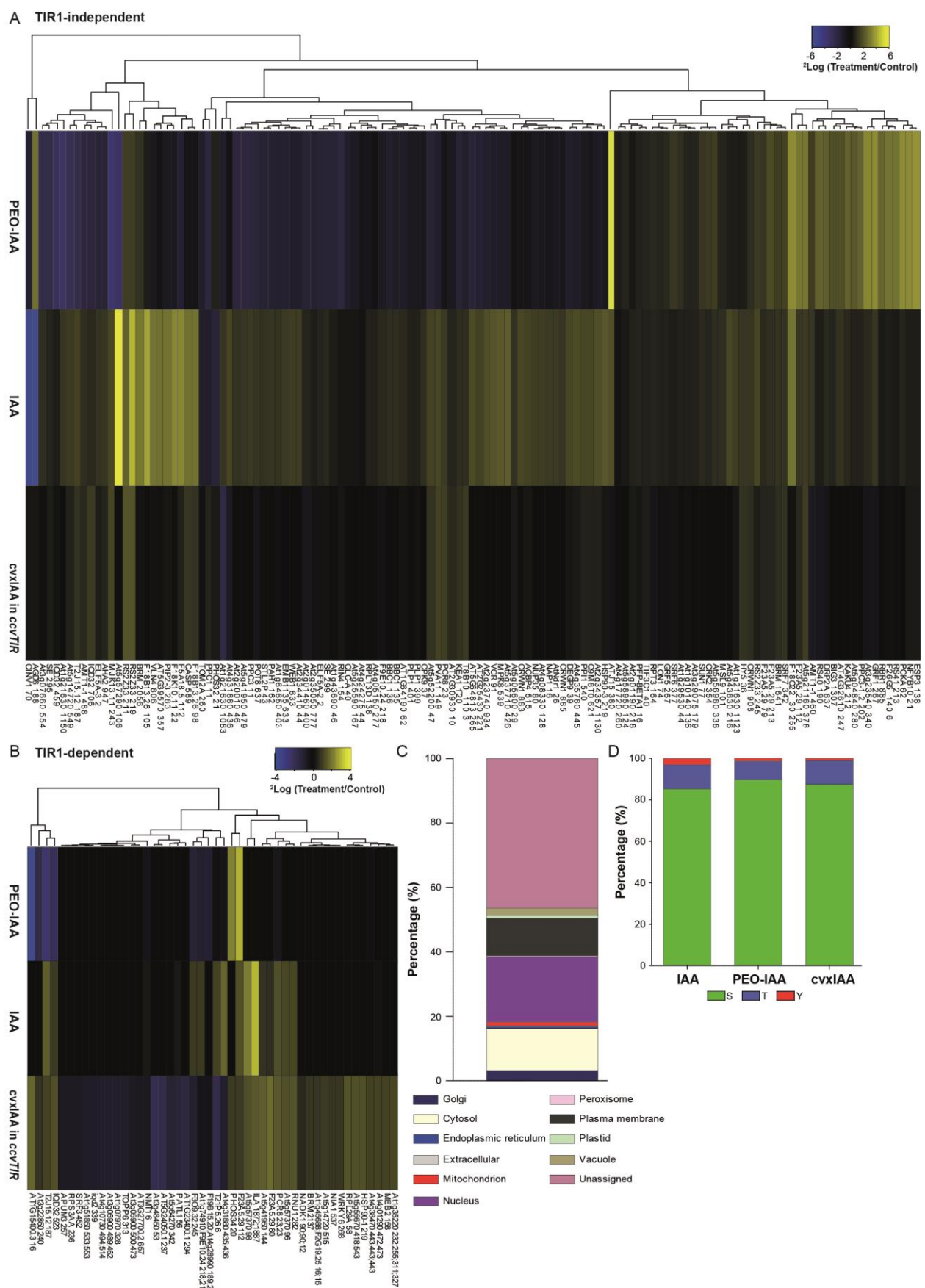
856 **Figure S3. Conserved phosphorylation site in the myosin XI protein family.**
857 Protein alignment of the global tail sequence of Myosin XI proteins shows that the auxin-induced phospho-
858 site (S1234 in Myosin XIK) is conserved.

```
XIG:  LAYWLTNTSALLFLLQKSLKPAGAGATASKKPPI-TTSLFGRMALSFRSSPNLAAAAEAAALAVIR
XIH:  LAYWLTNTSALLFLLQKSLKPAGAGATASKKPPI-TTSLFGRMALSFRSSPNLAAAAEAAALAVIR
XIB:  LAYWLTNTSALLFLLQKSLKPAGAGATASKKPPI-TTSLFGRMALSFRSSPNLAAAAEAAALAVIR
XIA:  LTNTSTLLFLLQRSLRQQSSTGSSPTKPPQ-----PTSFFGRMTQGFRSTSSPNLSTDVV
XID:  LAYWLTNTSTLLFLLQRSLKSHSTTGASPKKPPQP-TSFFGRMTQGFRSPSSASLSGDVV
XIF:  LYLLQSTLKFSNTNNAASRRNRSSHATLFGRLVQGMQPS---SVGLETSSGYSGMAGIPN
XI2:  LYLLQSTLKFSNTNNAASRRNRSSHATLFGRLVQGMQPS---SVGLETSSGYSGMAGIPNDQ
XIC:  LLLLQRTLKASGAAGMAPQRRRSSSATLFGRMSQSFRGAP---PGVNLAMINGAAGGGADTFR
XIE:  LLLLQRTLKASGAAGMAPQRRRSSSATLFGRMTQSFRGTP---QGVNLAMINGGVDTL
XIK:  LLLLQRTLKATGAASLTPQRRRTTSASLFGRMSQGLRGSP---QSAGLSFLNRQGLTKLDDLR
XI1:  LQRTLKAGATGSITTPRRRGM-PSSLFGRVSQSFRGSP-----QSAGFPFMTGRAIGGGLDELR
XII:  LRSNSFLNASAQRSGRAAYGVKSPFKL-HGPDDGASHIEARYPALLFKQQLTACVEKIYGLIRD
```

859 **Figure S4. Auxin and trafficking response in phospho-deficient myosin mutants (WT background).**

860 (A-C) Phosphorylation of Myosin XI phospho-deficient proteins (resp. *XIF^{S1256A}* and *XIK^{S1234A}*) following

861 auxin treatment visualized by Western and Phos-tag blot assays. 7 days old whole seedlings were treated

862 with 10 µM NAA or mock (DMSO solvent) for 30 minutes. Proteins were extracted of whole seedlings and

863 submitted to Western and Phos-tag blot analysis. The anti-actin loading control within the same sample

864 lane was used to normalize the protein expression level. In these lines, the anti-RFP antibody picks up

865 multiple bands in the Phos-tag gels, for which the intensity was not increased upon auxin treatment as was

866 the case for WT proteins (**Figure 2C-D**).

867 (D) Representative images showing the effect of BFA and the BFA + NAA co-treatment in XIF^{WT} and

868 XIF^{S1256A} mutants in WT background. 3 days old seedlings were pre-treated with 10 µM NAA or DMSO

869 mock for 30 minutes and then co-treated with 50 µM BFA + 10 µM NAA for an additional 60 minutes.

870 Seedlings were immunostained using anti-PIN1 according to Sauer et al. (2006). Scalebar = 10 µm.

871 (E) Representative confocal images of FM4-64 staining in MyosinXIF^{WT} and phospho-deficient XIF^{S1256A}

872 roots (in WT background). Cytoplasmic (CM) and PM staining were observed in 4 days old seedlings

873 treated with 10 µM NAA or DMSO mock for 30 minutes followed by 2 µM FM4-64 staining. Scale bar =
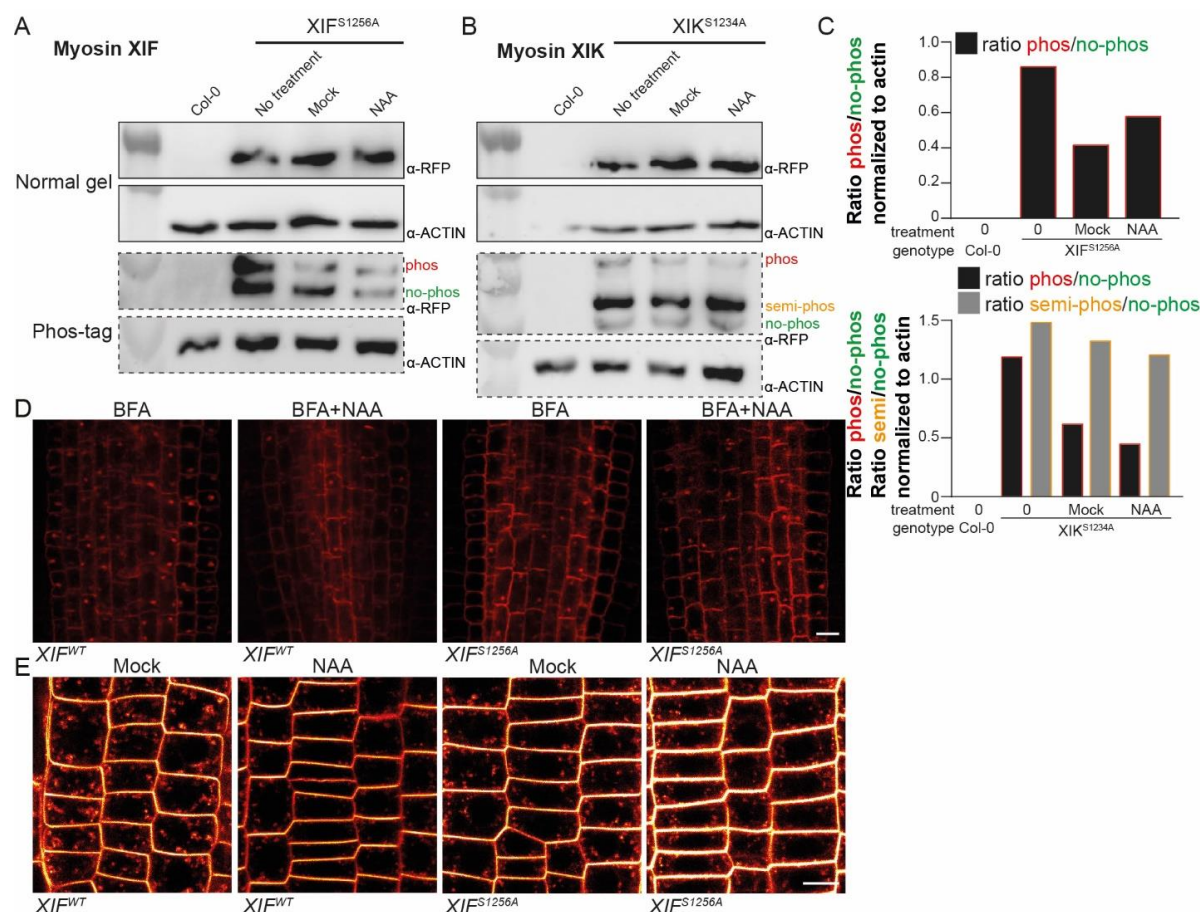
874 10 µm.

Figure S5: Endomembrante trafficking in phospho-deficient and phospho-mimic mutants (in *myosin xik xif* background)

(A) Representative images demonstrating the effect of BFA treatment or the co-treatment BFA + NAA in roots over-expressing XIF^{WT} and XIF^{S1256A} in *myosin xik xif* mutant background. 3 days old seedlings were pre-treated with 10 µM NAA or DMSO mock for 30 minutes and then co-treated with 50 µM BFA and 10 µM NAA for another 60 minutes followed by anti-PIN1 antibody immunostaining according to Sauer et al. (2016). Scale bar = 10 µm.

(B) Representative images demonstrating the effect of BFA treatment or the co-treatment BFA + NAA in roots over-expressing XIK^{WT} and XIK^{S1234A} in *myosin xik xif* mutant background. 3 days old seedlings were pre-treated with 10 µM NAA or DMSO mock for 30 minutes and then co-treated with 50 µM BFA and 10 µM NAA for another 60 minutes followed by anti-PIN1 antibody immunostaining according to Sauer et al. (2016). Scale bar = 10 µm.

(C) Quantification of BFA bodies in WT, *myosin xik xif* and phospho-deficient XIF^{S1256A} and XIK^{S1234A} roots (**Figure S5A-B**). The average number of BFA bodies was determined per root, including a correction for the total number of cells evaluated per root. n > 20. Bars represent the mean ± SD. **** for p ≤ 0.0001 and ns for p >0.05 determined by Tukey's multiple comparison test.

(D) Representative confocal images of FM4-64 staining in roots over-expressing XIF^{WT} and XIF^{S1256A} (in *myosin xik xif* background). PM staining and internalization of FM4-64 staining was imaged in 4 days old seedlings treated with 10 µM NAA or DMSO mock for 30 minutes. Scale bar = 10 µm.

(E) Representative confocal images of FM4-64 staining in roots over-expressing XIK^{WT} and XIK^{S1234A} (in *myosin xik xif* background). PM staining and internalization of FM4-64 staining was imaged in 4 days old seedlings treated with 10 µM NAA or DMSO mock for 30 minutes. Scale bar = 10 µm.

(F) Quantification of FM4-64 staining in WT, *myosin xik xif* and all phospho-deficient roots (**Figure S5C-D**). The CM/PM ratio was calculated by dividing the internal staining intensity by the PM-intensity. Bars represent the mean ± SD. Observations were made in more than 50 cells in more than10 different roots. *** for p ≤ 0.001 and **** for p ≤0.0001 determined by Tukey's multiple comparison test.
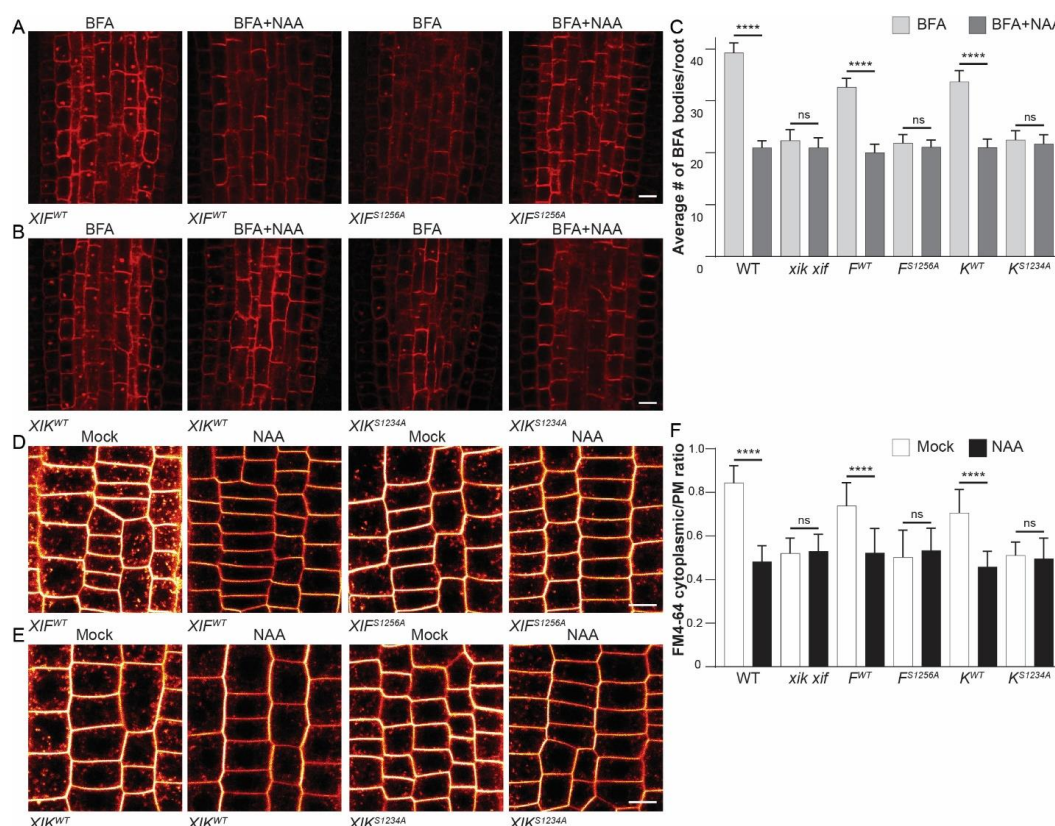
Figure S6. Auxin-induced PIN1 lateralization in WT and phospho-deficient MyosinXI constructs (in WT and in *myosin xik xif* background).

(A) PIN1 imunolocalization in WT roots transformed with resp. XIF^{WT}, XIF^{S1256A} and XIK^{WT}. Arrowheads indicate the predominant PIN1 localization in the endodermal cells. Scale bar = 10 µm.

(B) PIN1 imunolocalization in *myosin xik xif* mutant roots transformed with resp. XIF^{WT} and the phospho-deficient Myosin XIF construct (XIF^{S1256A}). Arrowheads indicate the predominant PIN1 localization in the endodermal cells. Scale bar = 10 µm.

(C) PIN1 imunolocalization in *myosin xik xif* mutant roots transformed with resp. XIK^{WT} and the phospho-deficient Myosin XIK construct (XIK^{S1234A}). Arrowheads indicate the predominant PIN1 localization in the endodermal cells. Scale bar = 10 µm.

(D) Quantification of auxin-mediated PIN1 lateralization in *myosin xik xif* mutants transformed with the different non-mutated and phospho-deficient MyosinXIF and XIK constructs (**Figure S6B-C**). The ratio was calculated by dividing the PIN1 intensity signal of the lateral side of versus the basal side of the respective endodermal cells. Data represent the mean ± SD. n = 15, more than 50 cells were quantified. **** p ≤0.0001 determined by Tukey's multiple comparison test.
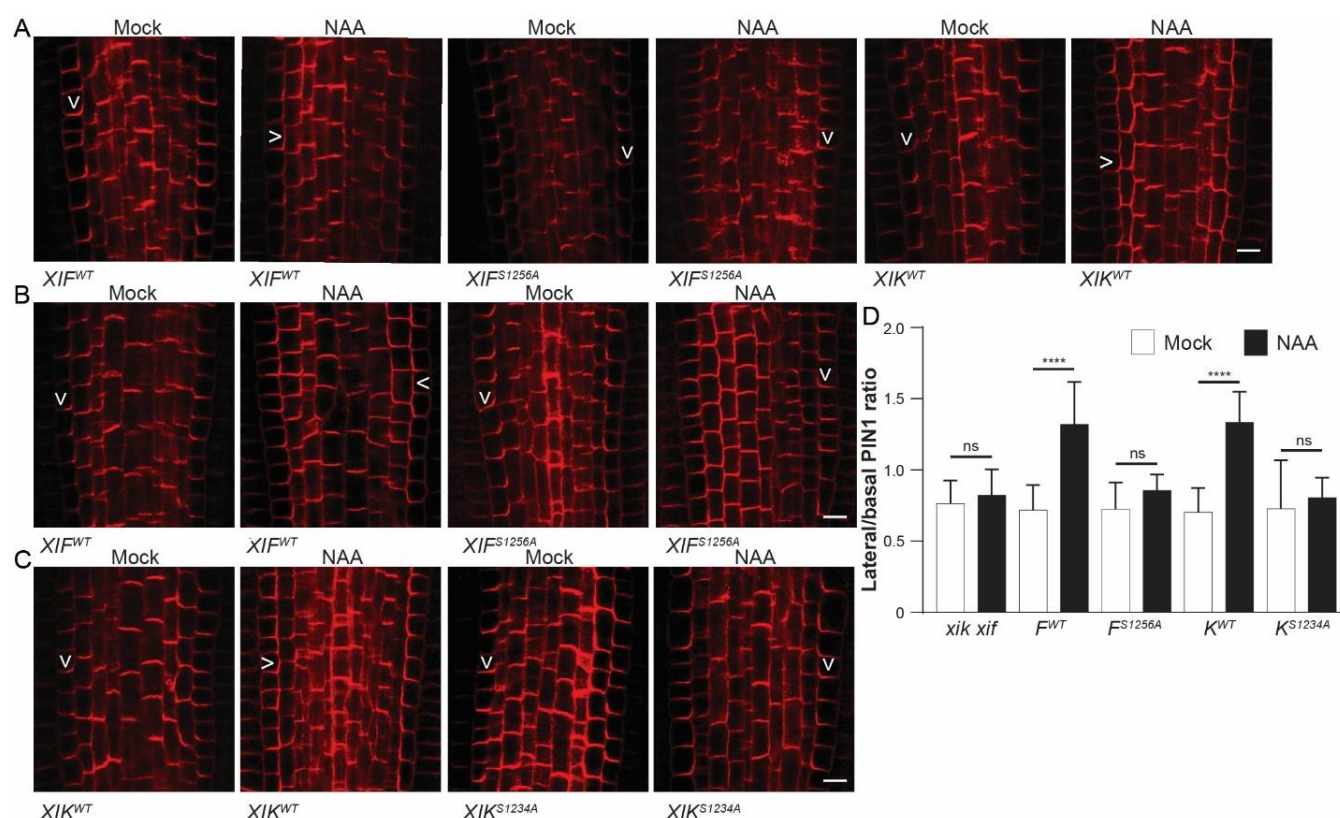
916 **Figure S7. The Madb2 myosin binding protein contributes to PIN trafficking and polarity regulation.**
917 (A) Representative images and quantification demonstrating the effect of BFA treatment or the co-treatment
918 BFA + NAA in *madb2 4KO* mutant roots. 3 days old seedlings were pre-treated with 10 µM NAA or DMSO
919 mock for 30 minutes and then co-treated with 50 µM BFA and 10 µM NAA for another 60 minutes followed
920 by anti-PIN1 antibody immunostaining according to Sauer et al. (2016). Scale bar = 10 µm. The average
921 number of BFA bodies was determined per root, including a correction for the total number of cells
922 evaluated per root. n > 20. Average # of BFA bodies per root ± SD is represented. **** for p ≤ 0.0001 and
923 ns for p >0.05 determined by Tukey's multiple comparison test.
924 (B) Representative confocal images and quantification of FM4-64 staining in *madb2 4KO* roots. PM
925 staining and CM internalization of FM4-64 staining were imaged in 4 days old seedlings treated with 10
926 µM NAA or DMSO mock for 30 minutes. Scale bar = 10 µm. The CM/PM ratio was calculated by dividing
927 the internal staining intensity by the PM-intensity. Bars represent the mean ± SD. *** for p ≤ 0.001 and
928 **** for p ≤0.0001 determined by Tukey's multiple comparison test.
929 (C) Representative images and quantification of PIN1 localization in *madb 4ko* mutant roots upon 10 µM
930 NAA-treatment. To visualize the auxin-induced lateralization, the intensity ratio of lateral to basal PIN1
931 signal was calculated per cell. Whereas 10 µM NAA in WT resulted in lateralization of PIN1 in root
932 endodermal cells, this effect was missing in *madb 4KO* mutant roots. Data represent the mean ± SD. More
933 than 50 cells were evaluated in at least 15 independent roots. **** p ≤0.0001 determined by Tukey's
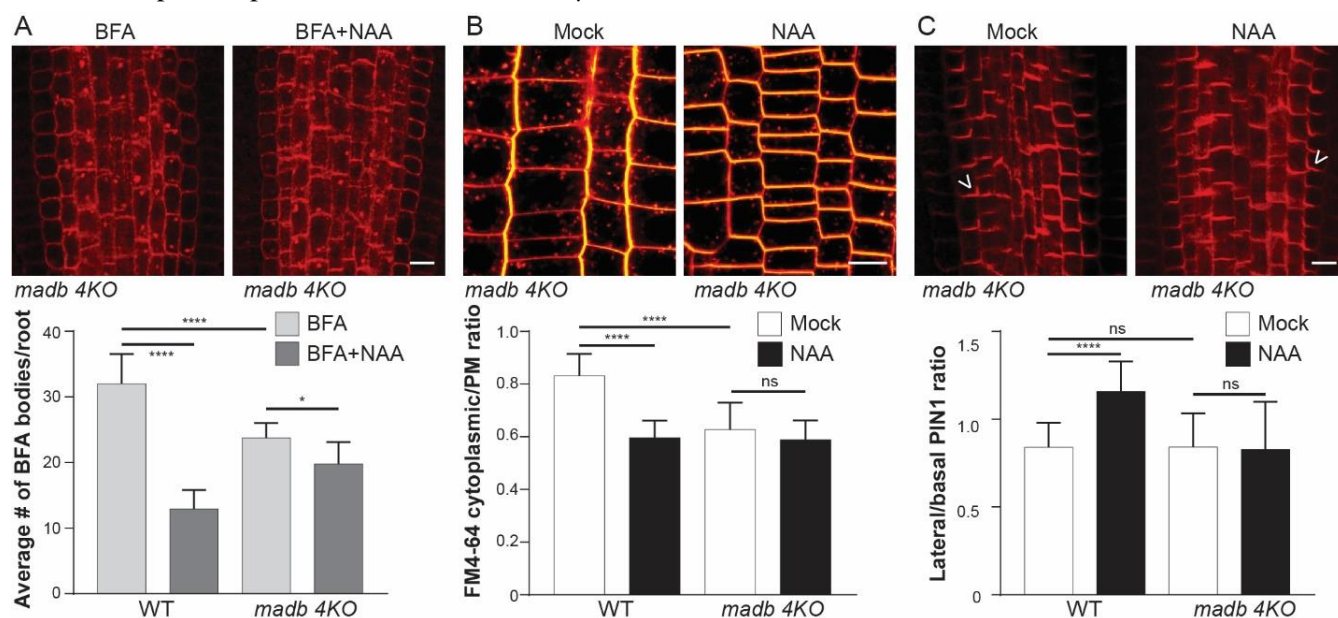934 multiple comparison test. Scale bar = 10 µm

Figure S8. Auxin-induced PIN3 polarization in phospho-deficient myosin mutants in WT background.

(A) Representative images showing PIN3-GFP localization hypocotyls expressing the non-mutated Myosin XIF/XIK and the phospho-deficient MyosinXIF^{S1256A} and MyosinXI^{KS1234A} constructs upon DMSO or NAA treatment. Arrowheads indicate PIN3 at outer side of hypocotyl endodermal cells. Scale bar = 25 µm.

(B) Polar auxin transport (PAT) in *myosin xik xif* mutant hypocotyls is decreased in comparison to WT, but not as significant as in the NPA-treated hypocotyls. Averages of 3 independent biological repeats existing of 15 hypocotyls ± SD are represented. * p ≤ 0.05 and **** p ≤0.0001 determined by Student t-tests compared to WT.(C) Representative seedlings showing gravity-induced hypocotyl bending of the WT MyosinXIF and XIK constructs compared to their phospho-deficient versions, resp. XIF^{S1256A} and XIK^{S1234A} expressed in *myosin xik xif* mutant background.

(C) Representative images of cotyledon vasculature patterns showing the normal venation pattern with 4 loops, less loops and cotyledons with more loops. Scoring of the number of loops was performed in cotyledons of WT, *myosin xik xif* and the different phospho deficient mutants (WT background). n > 50
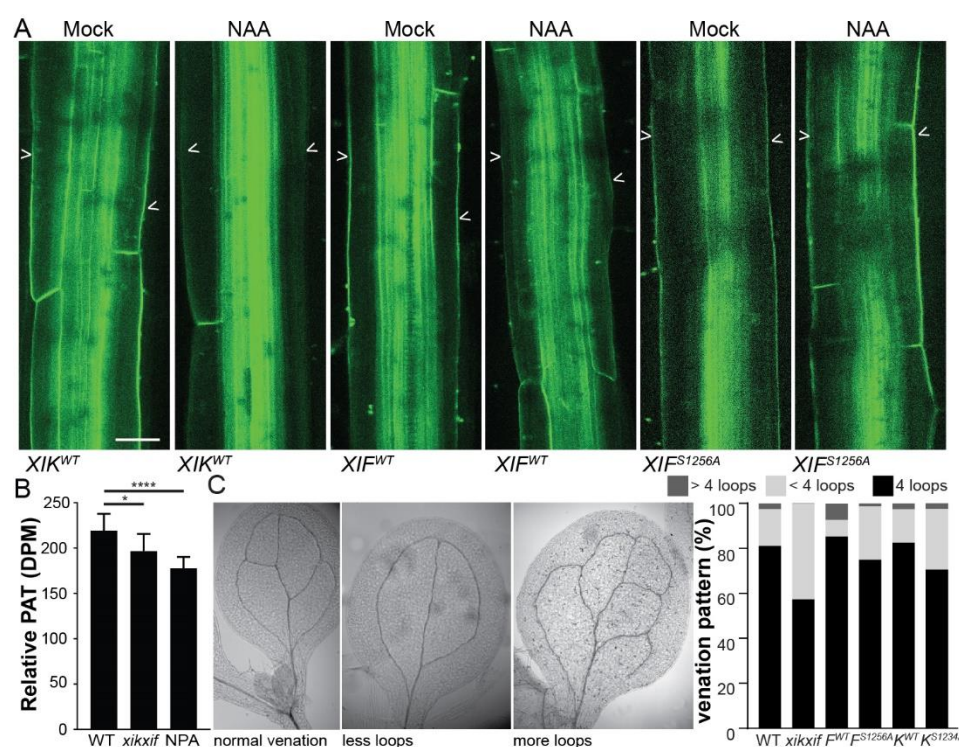
Figure S9. Gravity-induced PIN3 polarization in myosin mutants.

(A) Schematic changes of PIN3 in the hypocotyl upon gravity stimulation.

(B) Quantification of the bending response in WT, *myosin xik xif* and the lines expressing XIF^{WT}/XIK^{WT} and the phospho-deficient mutant versions (XIF^{S1256A} and XIK^{S1234A}). PIN3-GFP intensity at the lower and upper side of hypocotyl endodermal cells is represented. The start ratio at t0 is compared to the ratio after 6 and 24h of gravistimulation. At least 20 hypocotyls were evaluated **** p ≤0.0001 determined by Tukey's multiple comparison test.

(C) Representative images of PIN3-GFP localization in gravity-stimulated WT and *myosin xik xif* hypocotyls, 6h and 24h after the gravity switch. In all genotypes the 6h response was normal, with an increased lower/upper endodermal PIN3-GFP ratio. However, in 24h gravity-stimulated *myosin xik xif* hypocotyls and hypocotyls expressing the phospho-deficient XIF^{S1256A} and XIK^{S1234A} versions, no re-establishment of PIN3-GFP balance was observed, indicating that there are problems in the termination of the gravity response, explaining the hyperbending observed in these lines (**Figure 6B**). Arrowheads indicate the outer side of hypocotyl endodermal cells. Scale bar = 20 µm.
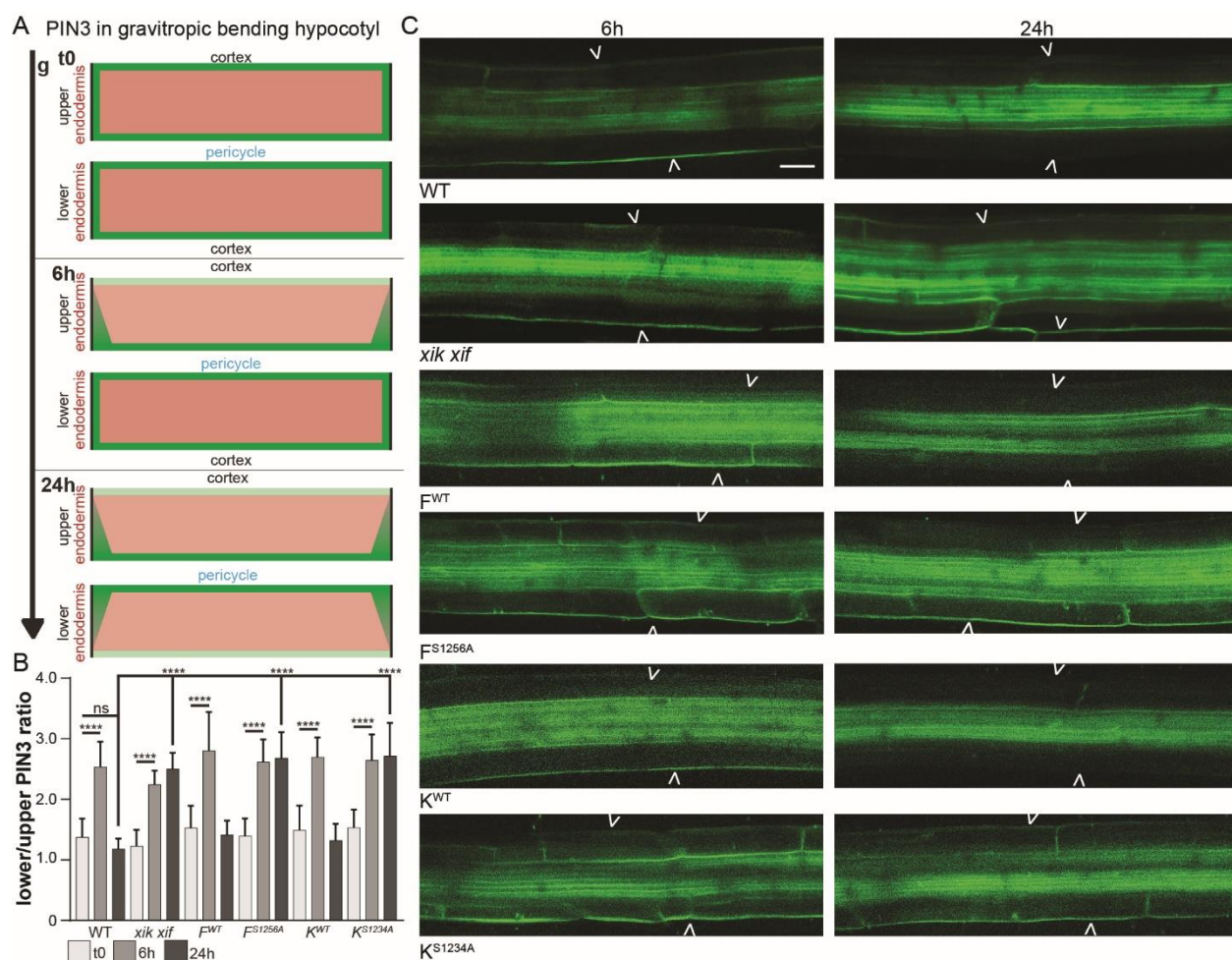
Supplemental Table 1

Table contains analyzed differentially regulated phosphopeptides (FDR ≤0.05) data of IAA, PEO-IAA and cvxIAA treatments.

Methods

Plant material and growth

The following transgenic and mutant lines were used: WT (Col-0), *pPIN3::PIN3-GFP* (Žádníková et al., 2010), *myosin xik xif* (Okamoto et al., 2015), *madb 4KO* (Kurth et al., 2017). Mutant combinations in *PIN3::PIN3-GFP* were generated through genetic crosses. Seeds were surface-sterilized by chlorine gas, sown on half-strength Murashige and Skoog (½ MS) medium supplemented with 1% (w/v) sucrose and 0.8% (w/v) phyto agar (pH 5.9), stratified in the dark at 4°C for 2 days and then grown vertically at 21°C with a long-day photoperiod (16h light/8h dark). Light sources used were Philips GreenPower LED production modules [in deep red (660 nm)/far red (720 nm)/blue (455 nm) combination, Philips], with a photon density of 140.4 µmol/m^2/s ± 3%.

Protein extraction

Five days after germination, roots were treated with either 100 nM IAA, 10 µM PEO-IAA or 1 µM cvxIAA or their respective solvents as mock. Root tips were directly harvested on liquid nitrogen. For IAA and PEO-IAA treatments, Col-0 WT was used, while for cvxIAA treatment, *ccvTIR1* seeds were used (Uchida et al., 2018). The harvested root tips were ground to fine powder in liquid nitrogen and extracted in SDS lysis buffer (100mM Tris pH8.0, 4%SDS and 10mM DTT). Protein extract was sonicated using a cooled Biorupter (Diagenode) for 10 minutes using high power with 30 seconds on 30 seconds off cycle. The lysate was cleared by centrifugation at maximum speed (13,000xg) for 30 minutes. Protein concentrations were determined using Bradford reagent (Bio-Rad).

Protein precipitation

Acetone precipitation was done according to Humphrey et.al. (2015). Methanol chloroform precipitation was done according to Vu et.al. (2016). For trichloroacetic acid (TCA) precipitation 1 volume of ≥99% TCA was added to 4 volumes of protein lysate. Mixtures were incubated on ice for 10 minutes and spun at maximum speed (13,000xg) for 5 minutes at 4°C. Pellet was washed twice with acetone at maximum speed (13,000xg) for 5 minutes at 4°C and then air dried and resuspended in 50 mM ammoniumbicarbonate (ABC) (Sigma).

Filter aided sample preparation (FASP)

For FASP, 30 kDa cut-off amicon filter units (Merck Millipore) were used. Filters were first tested by applying 1000 µl urea buffer UT buffer (8 M Urea and 100mM Tris, pH 8.5) and centrifuging for 20 minutes at 6,000 RPM. All further centrifuging steps were at this speed and temperature. The desired amount of protein sample was next mixed with UT buffer to a volume of 5000 µl, applied to filter and centrifuged for

1001 20 minutes. Filter were washed with UT buffer and centrifuged for 20 minutes. Retained proteins were

1002 alkylated with 50 mM acrylamide (Sigma) in UT buffer for 30 minutes at 20°C while gently shaking. Filter

1003 was centrifuged and afterwards washed three times with UT buffer for 20 minutes. Next, filters were washed

1004 three times with 50 mM ABC buffer. After the last wash, proteins were cleaved by adding Trypsin (Roche)

1005 in a 1:100 trypsin:protein ratio. Digestion was completed overnight. Filter was transferred to a new tube

1006 and peptides were eluted by 20 minutes centrifugation. Further elution was completed by two times adding

1007 50 mM ABC buffer and centrifuging.

1008

1009 **C18 Stage tip clean up**

1010 For peptide desalting and concentrating, 1000 µl tips were fitted with 2 plugs of C18 octadecyl 47mm Disks

1011 2215 (Empore™) material and 10 μg of LiChroprep® RP-18 peptides (Merck). Tips were sequentially

1012 equilibrated with 100 % methanol, 80 % ACN in 0.1 % formic acid and twice with 0.1 % formic acid with

1013 intermitting centrifuging for 4 minutes at 1,500xg. After equilibration, peptides were loaded and centrifuged

1014 for 20 minutes at 400xg. Bound peptides were washed with 0.1 % formic acid and eluted with 80 % ACN

1015 in 0.1 % formic acid by spinning for 4 minutes at 1,500xg. Eluted peptides were subsequently concentrated

1016 using a vacuum concentrator for 30 minutes at 45°C and resuspended in 50 µl 0.1 % formic acid.

1017

1018 **Phosphopeptide enrichment**

1019 For the magnetic Ti^{4+}-IMAC (MagResyn) and TiO_2-MOAC (MagResyn) approaches, the manufacture's

1020 protocols were followed without modifications (Resyn Biosciences). For stage tip based TiO_2

1021 Titansphere™ (GL Sciences) a 1:2 peptide to TiO_2 (µg/µg) was used. FASP eluted peptides were mixed

1022 with ACN and TFA to a concentration of 50 % ACN and 6 % TFA. TiO_2 columns were made with double

1023 C8 membrane and desired amount of beads in 100 % methanol. The columns were washed and equilibrated

1024 with 100 % ACN and 80 % ACN in 6 % TFA using centrifugation for 4 minutes at 1,500xg. Sample was

1025 loaded at 400xg for 30 minutes. Non-specifically bound peptides were washed with 80 % ACN in 6 % TFA

1026 by centrifugation for 4 minutes at 1,500xg and 2 times with 60 % ACN in 1 % TFA for 4 minutes at 1,500xg.

1027 Next, bound phosphopeptides were eluted three times in 40 % ACN and 15 % NH_4OH. After the last elution

1028 samples were concentrated using a vacuum concentrator for 30 minutes at 45°C. Samples were subsequently

1029 acidified using 10% TFA and processed with C18 Stagetip clean up.

1030

1031 **Mass spectrometry and data analysis**

1032 Phosphopeptides were applied to online nanoLC-MS/MS using a 120 min acetonitrile gradient from 8-50 %.

1033 Spectra were recorded on a LTQ-XL mass spectrometer (Thermo Scientific) according to Wendrich et.al.

1034 (2017). Data analysis of obtained spectra was done in MaxQuant software package (Wendrich et al., 2017),

1035   with the addition of phosphorylation as a variable modification. Data analysis and visualization was

1036   performed in Perseus, Adobe Illustrator and R. Filtering of phosphopeptides was conducted using a hybrid

1037   data filtering approach as described previously (Nikonorova et al. 2018). Protein subcellular localisation

1038   analysis was preformed using the Multiple Marker Abundance Profiling (MMAP) tool on the subcellular

1039   localisation database for Arabidopsis proteins (SUBA4) (Hooper et.al. 2017).

1040

1041   **Myosin XIK and XIF phosphorylation mutagenesis**

1042   The Myosin XIK and XIF GTD sequences (from amino acid 1100 to the C terminus) (Peremyslov et al.,

1043   2008) with mutations S1234A (XIK^{S1234A}), S1256A (XIF^{S1256A}) or in non-mutated version (XIK^{WT} and XIF^{WT})

1044   were synthesized and recombined into the pDONR221 Gateway vector and the pB7RWG2 expression

1045   vector. All the constructs were re-sequenced to confirm the mutation sites and transformed into *Arabidopsis*

1046   plants (WT and *myosin xik xif* mutant background) using flower dip method.

1047

1048   **Protein extraction and immunoblot assay**

1049   7 days old homozygous T3 seedlings of XIK^{WT}, XIK^{S1234A}, XIF^{WT} and XIF^{S1256A} expressing lines were treated

1050   with DMSO or 10 µM NAA for 30 minutes and full seedlings were harvested. Samples were frozen in

1051   liquid nitrogen, ground into powder and homogenized in protein extraction buffer (50 mM Tris-HCl,

1052   pH=7.5; 150 mM NaCl; 0.15% NP40; 10 mM DTT (1, 4-dithiothreitol); 1 mM PMSF; containing protease

1053   inhibitor and phosphatase inhibitor). After 20 minutes of centrifugation (16,000 *g*) at 4 °C, total protein

1054   extract was collected and concentration was determined by Bradford Reagent (Bio-Rad). Lambda protein

1055   phosphatase treatment (New England BioLabs) was performed following the manufactorer's protocol.

1056   After adding an equal amount of loading buffer (4× Laemmli Sample Buffer, Bio-Rad), an equivalent of

1057   30 µg total protein for each sample was boiled at 65°C for 10 minutes and then separated on a 10% normal

1058   or the Phos-tag SDS-PAGE (Phos-tag acrylamide AAL-107, Wako Pure Chemical Industries, #304-93521).

1059   Proteins were transferred to a PVDF membrane by wet blotting. The membranes were incubated with

1060   primary rat monoclonal anti-5F8 antibody (Chromotek, 1:1000) and secondary bovine anti-rat horseradish

1061   peroxidase (HRP)-conjugated (1:5000) antibody. Following detection of the myosin protein, the

1062   membranes were stripped and incubated with primary plant Monoclonal Anti-Actin (Sigma, A0480, 1:1000)

1063   and secondary anti-mouse HRP (1:500) antibody overnight. HRP activity was detected by the Supersignal

1064   Western Detection Reagents (Thermo Scientific) and imaged with a GE Healthcare Amersham 600RGB

1065   system.

1066

1067   **Quantification of hypocotyl gravitropic bending angle**

1068   To monitor gravitropic responses, plates with 3 days old etiolated seedlings were turned 90° compared to

1069   the original gravitropic vector. The plates were scanned 24 hours after gravistimulation and bending was

1070   recorded at 1 hour intervals. The hypocotyl bending angle was measured using ImageJ (NIH;

1071   http://rsb.info.nih.gov/ij).

1072

1073   **Quantitative analysis of PIN3-GFP polarization in hypocotyl**

1074   The *pPIN3::PIN3-GFP* intensity was measured using ImageJ in the hypocotyl as described previously

1075   (Rakusová et al., 2019). After gravity stimulation, the ratio between lower and upper side endodermal cells

1076   was calculated. For auxin treatment, 3 days old etiolated seedlings were transferred to new plates with 10

1077   µM of NAA, or the equivalent amount of DMSO for 4 hours in darkness after which the inner/outer ratio

1078   was calculated for the relevant endodermal cells.

1079

1080   **Hypocotyl basi-petal auxin transport assay**

1081   6 days etiolated seedlings were transferred to new ½ MS plates. 3 replicates of 15 seedlings for each mutant

1082   or treatment were used. ^{3}H-IAA was added into ½ MS medium (1.25% phyto-agar) to a final concentration

1083   of 1.5 µM. From this agar solution, a 5 µl ^{3}H-IAA droplets was made and once solidified, this droplet was

1084   placed on the top of the hypocotyl from which the cotyledons were excised. During the following 6 hours

1085   the seedlings were kept in the dark. 10 µM *N*-1-Naphthylphthalamic acid (NPA) in the droplets was used

1086   as a control. After 6 hours, the roots and the top of the hypocotyl, which was in contact with the droplet

1087   were removed. The remaining hypocotyl samples were homogenized in liquid nitrogen and incubated

1088   overnight in Opti-Fluor Scintillation Cocktail (Perkin Elmer). The amount of ^{3}H-IAA taken up by the

1089   hypocotyl was measured in a scintillation counter (Hidex 300SL) and this represents basipetal polar auxin

1090   transport (PAT). Measurements were performed in three technical and three biological replicates.

1091

1092   **Leaf venation assay**

1093   7 days old light grown seedlings were used for leaf venation analysis. Cotyledons were cleared in 4% HCl

1094   and 20% methanol for 15 minutes at 65°C, followed by a 15 minutes incubation in 7% NaOH and 70%

1095   ethanol at room temperature. Next, seedlings were rehydrated by successive incubations in 70%, 50%, 25%,

1096   and 10% ethanol for 5 minutes each, followed by incubation in 25% glycerol and 5% ethanol for 2 days at

1097   room temperature. Finally, cotyledons were mounted in 50% glycerol and were monitored by differential

1098   interference contrast DIC microscopy (Olympus BX53). The cotyledon venation pattern was evaluated by

1099   counting the number of loops and defects such as open loops, extra branches and disconnectivity were

1100   scored.

1101

Regeneration of stem after wounding

For the regeneration experiments, young, approximately 10 cm tall *Arabidopsis thaliana* inflorescence stems were tranversally cut at the base, 3 to 4 mm from the rosette. This transversal incission interrupts the longitudinal continuum of vascular cambium and secondary tissues and hence the ongoing transport. Plants were covered with an artificial weight according to Mazur et al. (2016). Axillary buds growing above the rosette were not removed, thereby mainting a source of endogenous auxin. 7 days after wounding, the stem segments were sectioned to 80 µm native sections using an automated vibratome (Leica VT1200 S, Leica Mycrosystems Ltd., Wetzlar, Germany). These sections were stained with a 0.025 % Toluidine Blue O and regeneration was analyzed in stems by observations using a wide field microscope at 10x magnification (Zeiss Axioscope.A1 ZENAxiocam 105).

Auxin-induced canalization in wounded inflorescence stems.

Arabidopsis plants with young, 10 cm tall inflorescence stems were chosen for exogenous auxin application. Stems were wounded by a transversal incision 3-4mm above the rosette to interrupt the vascular cambium and secondary tissues and hence also the polar, basipetal transport of endogenous auxin. We then applied 10 µM IAA (Sigma-Aldrich, cat. no 15148-2G) in a droplet of lanoline paste below the cut. This droplet was replaced every 2 days to ensure the constant presence of auxin. Samples were collected and the manual longitudinal stem sections were obtained under a NIKON MSZ1500 stereomicroscope. Sections were stained in 0,05% Toluidine Blue O and mounted in a 50% glycerol aqueous solution. Images of these sections were obtained by the Olympus BX43 microscope equipped with an Olympus SC30 Camera. n = 20

Whole-mount *in situ* immunolozalization

For PIN1 localization in root, 3 days old primary roots were treated for 4h with 10 µM of NAA in liquid ½ MS medium. Immunolozalization and quantificaiton of PIN1 lateralization were carried out as described previously (Sauer et al., 2006). The following antibodies were used: anti-PIN1 (1:1000), secondary goat anti-rabbit antibody coupled Cy3 (Sigma-Aldrich, 1:600). PIN1 localization was monitored by LSM 800 microscopy.

FM4-64 uptake assay

4 days old light grown seedlings were incubated with 10 µM NAA or the equivalent amount of DMSO for 30 minutes in ½ MS liquid medium. Then 2 µM FM4-64 was added to the medium for 15 minutes and roots were mounted and observed using a LSM-800 Zeiss confocal microscope. Signal intensity at PM and

1135   cytoplasm (CP) was measured using ImageJ. The ratio between CP and PM was calculated and statistical

1136   analysis was performed in GraphPad Prism.

1137

1138   **BFA treatment assay**

1139   To monitor PIN1 trafficking in the root, 3 days old light grown seedlings were pretreated with 10 µM NAA

1140   or the equivalent amount of DMSO in ½ MS liquid medium for 30 minutes, and then co-treatment with 50

1141   µM BFA for another 60 minutes. Immunolozalization was carried out as described previously (Sauer et al.,

1142   2006). The average number of BFA bodies per root was quantified in the different mutant lines.

1143

1144   **Statistical analysis**

1145   All statistical analysis was done in GraphPad Prism (version 8.3.0(538)) and significant differences were

1146   determined using Anova Tests – Tukey for multiple comparisons. For all graphs the number of * indicate

1147   significance according to the following p-values: ns for $p > 0.05$, * for $p \leq 0.05$, ** for $p \leq 0.01$, *** for p

1148 ≤ 0.001.